HHS Public Access

Author manuscript

Nat Immunol. Author manuscript; available in PMC 2022 August 21.

Published in final edited form as:

Nat Immunol. 2022 March ; 23(3): 386–398. doi:10.1038/s41590-022-01131-3.

Tcf1 preprograms the mobilization of glycolysis in central memory CD8+ T cells during recall responses

Qiang Shan[1,7], **Shengen Shawn Hu**[2,7], **Shaoqi Zhu**[3], **Xia Chen**[1], **Vladimir P. Badovinac**[4], **Weiqun Peng**[3], **Chongzhi Zang**[2,5,8], **Hai-Hui Xue**[1,6,8]

[1]Center for Discovery and Innovation, Hackensack University Medical Center, Nutley, NJ 07110

[2]Center for Public Health Genomics, University of Virginia School of Medicine, Charlottesville, VA 22908

[3]Department of Physics, The George Washington University, Washington, DC 20052

[4]Department of Pathology, Carver College of Medicine, University of Iowa, Iowa City, IA 52242

[5]Department of Public Health Sciences, University of Virginia, Charlottesville, VA 22908

[6]New Jersey Veterans Affairs Health Care System, East Orange, NJ 07018

[7]These authors contributed equally to this work.

Abstract

The mechanisms underlying the heightened protection mediated by central memory $CD8^+$ T (T_{cm}) cells remain unclear. Here we show that the transcription factor Tcf1 was required in resting T_{cm} cells to generate secondary effector $CD8^+$ T cells and to clear pathogen during recall responses. Recall stimulation of $CD8^+$ T_{cm} cells caused extensive reprogramming of the transcriptome and chromatin accessibility, leading to rapid induction of glycolytic enzymes, cell cycle regulators and transcriptional regulators, including Id3. This cluster of genes did not require Tcf1 in resting $CD8^+$ T_{cm} cells, but depended on Tcf1 for optimal induction and chromatin opening in recall-stimulated $CD8^+$ T_{cm} cells. Tcf1 bound extensively to these recall-induced gene loci in resting $CD8^+$ T_{cm} cells, and mediated chromatin interactions that positioned these genes in architectural proximity with poised enhancers. Thus, Tcf1 preprogramed a transcriptional program that supported the bioenergetic and proliferative needs of $CD8^+$ T_{cm} cells in case of a secondary challenge.

$CD8^+$ T lymphocytes are essential for mounting protective cellular immune responses against pathogenic antigens and malignantly transformed cells[1, 2]. In acute viral or intracellular bacterial infections, fully differentiated cytotoxic effector $CD8^+$ T cells clear the pathogens, while a fraction of the antigen-specific $CD8^+$ T cells differentiate into

[8]Corresponding authors: Hai-Hui Xue (Contact), 111 Ideation Way, Bldg. 102, Rm. A417, Nutley, NJ 07110, Tel: 201-880-3550; haihui.xue@hmh-cdi.org; Chongzhi Zang, 1335 Lee St. MSB 3235, Charlottesville, VA 22908, Tel: 434-243-5397; zang@virginia.edu.

Author contributions

Q.S. and X.C. performed the experiments and analyzed the data. S.S.H. analyzed the ChIP-seq, RNA-seq and ATAC-seq data under supervision of C.Z., S.Z. analyzed the Hi-C data under supervision of W.P., V.P.B. provided key reagents and scientific input. H.H.X. conceived the project and supervised the overall study. H.H.X. and C.Z. wrote the paper and all authors edited the paper.

memory CD8$^+$ T (T_m) cells. CD8$^+$ T_m cells consist of heterogeneous subsets, with distinct distribution patterns and functionality[3]. Unlike CD69$^+$CD103$^+$ resident and CD62L$^-$ effector T_m cells, CD62L$^+$ central memory CD8$^+$ T (T_{cm}) cells are more enriched in the lymphoid organs and possess the most robust proliferative capacity in response to restimulation. CD8$^+$ T_m, especially T_{cm} cells, have two cardinal features that resemble stem cells: self-renewal to maintain a stable CD8$^+$ T_m cell pool over time and differentiation into secondary effector CD8$^+$ T cells upon re-encountering the same antigen. The latter is conventionally known as T_m cell-mediated recall response, which is accelerated in time and increased in magnitude during differentiation to secondary effectors, hence conferring enhanced protection against the same pathogen.

The self-renewal of CD8$^+$ T_m cells depends on extrinsic input and intrinsic factors. Whereas CD8$^+$ T_m cell persistence does not depend on cognate antigens, they require homeostatic cytokines including IL-7 and IL-15 (ref.[4]). Several transcription factors, such as Eomes, Tcf1 and Foxo1, are essential intrinsic regulators of longevity of CD8$^+$ T_m cells[5, 6, 7, 8]. CD4$^+$ T cell-mediated help is essential for CD8$^+$ T_m cells to acquire the capacity to robustly respond to restimulation[9]. In terms of transcription regulators, deficiency in Tcf1, Foxo1, Stat3, Zeb1 or Bach2 impairs generation of CD8$^+$ T_m cells and their recall responses[6, 7, 8, 10, 11, 12, 13, 14], while forced expression of Bcl6 or Id3 enhances secondary expansion of CD8$^+$ T_m cells[15, 16]. Notably, this insight mostly comes from studies using a heterogenous pool of CD8$^+$ T_m cells. A mechanistic understanding of how CD8$^+$ T_{cm} cells respond to secondary challenge is largely absent.

Tcf1 and its homologue Lef1 have versatile roles in T cell biology, from T cell development to the differentiation of various CD4$^+$ helper lineages and CD8$^+$ subsets[17, 18, 19]. Tcf1 is highly expressed in naïve CD8$^+$ T cells, but greatly downregulated in fully differentiated effector CD8$^+$ T cells[20, 21]. CD8$^+$ T_m cells partly retain or regain Tcf1 expression, which is higher in CD8$^+$ T_{cm} than T_{em} cells[22]. Studies in germline-targeted mice suggest a contribution of Tcf1 to the recall capacity of unfractionated CD8$^+$ T_m cells[6, 10]. Here, we specifically ablated Tcf1 in activated CD8$^+$ T cells and used multi-omics approaches to mechanistically dissect the requirement for Tcf1 in the recall capacity of CD8$^+$ T_{cm} cells. Our observations indicated that Tcf1 preprogramed the mobilization of glycolysis in these cells to meet the bioenergetic needs associated with the rapid expansion of secondary effector CD8$^+$ T cells.

Results

Tcf1 and Lef1 regulate CD8$^+$ T_m cell fate redundantly

To bypass the requirements for Tcf1 and Lef1 in thymocyte development, we used mice transgenic (Tg) for *Gzmb-Cre*, which deletes target gene after CD8$^+$ T cell activation, Rosa26-STOP-GFP (*Rosa26*^{GFP}) mice, where GFP expression marks cells with *Gzmb-Cre*-mediated floxed gene deletion, and P14 TCR Tg mice, which express a TCR that specifically recognizes the glycoprotein 33–41 epitope (GP33) of lymphocytic choriomeningitis virus (LCMV). Through crossing with *Tcf7*- and/or *Lef1*-floxed alleles, we generated P14-Tg$^+$*Gzmb-Cre*$^+$*Rosa26*^{GFP}*Tcf7*$^{FL/FL}$ and P14-Tg$^+$*Gzmb-Cre*$^+$*Rosa26*^{GFP}*Tcf7*$^{FL/FL}$*Lef1*$^{FL/FL}$ mice (called *Tcf7*$^{\Delta Gzmb}$ and

Tcf7$^{\Delta Gzmb}$*Lef1*$^{\Delta Gzmb}$ hereafter), along with P14-Tg^{+}*Gzmb-Cre*$^{+}$*Rosa26*^{GFP} *Tcf7*$^{+/+}$ *Lef1*$^{+/+}$ wild-type littermate controls. We then adoptively transferred naïve wild-type, *Tcf7*$^{\Delta Gzmb}$ or *Tcf7*$^{\Delta Gzmb}$*Lef1*$^{\Delta Gzmb}$ CD45.2^{+}CD8^{+} T cells into wild-type CD45.1 recipients, followed by infection with LCMV Armstrong strain (LCMV-Arm) to elicit acute viral infection. *Gzmb-Cre* effectively deleted Tcf1 in activated CD8^{+} T cells, before first cell division (Extended Data Fig. 1a,b). At the peak response on day 8 post-infection (p.i.), expansion of *Tcf7*$^{\Delta Gzmb}$ primary effector CD8^{+} T cells was similar to that of wild-type CD8^{+} T cells, while the frequency and numbers of *Tcf7*$^{\Delta Gzmb}$*Lef1*$^{\Delta Gzmb}$ effector CD8^{+} T cells were modestly reduced compared to wild-type effector CD8^{+} T cells (Fig. 1a,b). The primary effector CD8^{+} T cell functions, such as production of IFN-γ, co-production of TNF and IL-2 and expression of granzyme B were minimally affected in *Tcf7*$^{\Delta Gzmb}$ CD8^{+} T cells, but were consistently decreased in *Tcf7*$^{\Delta Gzmb}$*Lef1*$^{\Delta Gzmb}$ CD8^{+} T cells compared to wild-type CD8^{+} T cells (Extended Data Fig. 1c–e). The generation of KLRG1^{lo}IL-7Rα^{+} memory precursor CD8^{+} T cells was not detectably affected by loss of Tcf1 alone, but was greatly diminished by ablating both Tcf1 and Lef1 (Fig. 1c,d). At the memory stage (≥day 30 p.i.)[23], the numbers and frequency of *Tcf7*$^{\Delta Gzmb}$ CD8^{+} T_m cells was reduced by ~50% compared to wild-type CD8^{+} T_m cells (Fig. 1e,f), while those of *Tcf7*$^{\Delta Gzmb}$*Lef1*$^{\Delta Gzmb}$ CD8^{+} T_m cells were almost negligible (Fig. 1f,g). Consistent with previous reports using *Tcf7*$^{-/-}$ mice[6, 10], *Tcf7*$^{\Delta Gzmb}$ CD8^{+} T cells generated fewer CD62L^{+} T_{cm} cells than wild-type CD8^{+} T cells (Fig. 1g,h). These observations indicate that Tcf1 and Lef1 functioned redundantly in determining the CD8^{+} T_m fate and generating CD8^{+} T_{cm} cells during the primary responses.

Tcf1 is essential for CD8^{+} T_{cm} cell recall responses

Because *Tcf7*$^{-/-}$ T_{cm} cell numbers decline over time[6], we focused on early memory phase to investigate how Tcf1 modulated the recall capacity of CD8^{+} T_{cm} cells. CD45.2^{+} CD8^{+}CD62L^{+} T_{cm} and CD62L^{-} T_{em} cells sorted from primary recipient mice set up as above at day 30–35 p.i. were adoptively transferred into CD45.1 wild-type recipients, followed by a secondary challenge with LCMV-Arm on the next day. At day 8 p.i., *Tcf7*$^{\Delta Gzmb}$ CD8^{+} T_{cm} cells gave rise to substantially fewer secondary effector CD8^{+} T cells than wild-type CD8^{+} T_{cm} cells, while *Tcf7*$^{\Delta Gzmb}$ and wild-type T_{em} cells generated similarly lower numbers of effector CD8^{+} cells compared to wild-type CD8^{+} T_{cm} cells (Fig. 2a). At 60 hours p.i., cell trace violet (CTV)-labeled wild-type CD8^{+} T_{cm} cells were mostly in divisions 5 and 6 after adoptive transfer and LCMV-Arm infection as above, while *Tcf7*$^{\Delta Gzmb}$ CD8^{+} T_{cm} cells were mostly in divisions 4 and 5 (Fig. 2b,c). Wild-type and *Tcf7*$^{\Delta Gzmb}$ CD8^{+} T_{cm} cells had a similar survival rate at this time point (Extended Data Fig. 2a). Additionally, wild-type and *Tcf7*$^{\Delta Gzmb}$ CD8^{+} T_{cm}-derived secondary effector CD8^{+} T cells had similar production of IFN-γ and TNF and expression of granzyme B at day 8 p.i. (Extended Data Fig. 2b–d). Upon adoptive transfer into *Tcra*$^{-/-}$mice (which lack T cells) followed by infection with *Listeria monocytogenes* expressing the GP33 epitope (LM-GP33), clearance of liver LM-GP33 was less efficient at day 5 p.i in recipients of *Tcf7*$^{\Delta Gzmb}$ CD8^{+} T_{cm} cells compared to those of wild-type CD8^{+} T_{cm} cells (Fig. 2d). Thus, Tcf1 critically regulated the differentiation of CD8^{+} T_{cm} cells to secondary effector CD8^{+} T cells.

Tcf1 predetermines CD8$^+$ T_{cm} gene induction by recall

CD8$^+$ T_{cm} cells rapidly mobilize cytotoxic machinery upon restimulation, and in fact, wild-type CD8$^+$ T_{cm} cells, but not naïve wild-type CD8$^+$ cells, produced IFN-γ after 24-hr *ex vivo* stimulation with GP33 (Fig. 3a)[24]. To capture the earliest molecular impact of Tcf1 deficiency on recall-stimulated CD8$^+$ T_{cm} cells, we performed RNA-seq in sorted wild-type and *Tcf7*$^{\Delta Gzmb}$ CD8$^+$ T_{cm} cells before and after 24-hr stimulation with GP33. Principal component analysis (PCA) showed that stimulation caused potent transcriptomic diversification from the resting state in wild-type and *Tcf7*$^{\Delta Gzmb}$ CD8$^+$ T_{cm} cells (Extended Data Fig. 3a). GP33 stimulation induced 3,144 genes and repressed 2,998 genes in wild-type CD8$^+$ T_{cm} cells (Fig. 3b). Comparison of wild-type and *Tcf7*$^{\Delta Gzmb}$ CD8$^+$ T_{cm} transcriptomes identified 458 differentially expressed genes (DEGs) before (Fig. 3c) and 795 DEGs after (Fig. 3d) GP33 stimulation, which collectively formed 4 major clusters based on their differential expression patterns (Fig. 3e). Genes in Cluster 3 and Cluster 4a were induced in GP33-stimulated wild-type CD8$^+$ T_{cm} cells, but showed impaired induction in GP33-stimulated *Tcf7*$^{\Delta Gzmb}$ CD8$^+$ T_{cm} cells (Fig. 3b,e). Functional annotation of these 'Tcf1-depedent, recall-induced T_{cm} genes' (Supplementary Table 1) indicated strong enrichment of "cell cycle", "DNA replication" and "ribonucleoprotein/protein translation" (Fig. 3f), consistent with the rapid secondary expansion of effector CD8$^+$ T cells, and enrichment of "mitochondria", "oxidative phosphorylation" and "glycolysis" (Fig. 3f), in line with the bioenergetics need during recall responses. Specifically, Cluster 3 and Cluster 4a included genes encoding multiple cyclins and cyclin-dependent kinases, transcriptional regulators of CD8$^+$ T cell responses such as *Id3*, *Irf8*, and *Ezh2*[16, 25, 26, 27] (Fig. 3g), and dozens of ATP synthases and cytochrome C oxidase subunits (Extended Data Fig. 3b). The 94 genes in Cluster 4a were downregulated in *Tcf7*$^{\Delta Gzmb}$ compared with wild-type CD8$^+$ T_{cm} cells at resting state, while the 530 genes in Cluster 3 were similarly expressed in resting wild-type and *Tcf7*$^{\Delta Gzmb}$ T_{cm} cells (Fig. 3e), suggesting Tcf1 was critical for preparing the CD8$^+$ T_{cm} cells for recall-stimulated gene induction. Cluster 1 genes were upregulated in *Tcf7*$^{\Delta Gzmb}$ compared to wild-type CD8$^+$ T_{cm} cells at resting state (Fig. 3c,e), and were enriched in functions such as "immunity", "defense to response to virus" (*Klrg1*, *Cd86* and *Prdm1*) and "lipid metabolic process" (*Pla2g15* and *Pld4*, encoding phospholipases A and D family members) (Extended Data Fig. 3c,d). However, most genes in Cluster 1 and Cluster 4b were similarly downregulated in wild-type and *Tcf7*$^{\Delta Gzmb}$ CD8$^+$ T_{cm} cells after GP33 stimulation (Fig. 3e, left columns). Cluster 2 genes were similarly expressed in resting wild-type and *Tcf7*$^{\Delta Gzmb}$ CD8$^+$ T_{cm} cells, but showed increased expression in GP33-stimulated *Tcf7*$^{\Delta Gzmb}$ compared to wild-type CD8$^+$ T_{cm} cells (Fig. 3e). These genes were enriched in functions including "cytokine-cytokine receptor interaction" (*Tnfsf10*, encoding TRAIL), "transcription regulation" (*Rel* and *Nfat5*) and "chromatin regulator" (*Dnmt3a* and *Kdm6b*) (Extended Data Fig. 3e,f); however, these genes were not known to impede CD8$^+$ T cell recall responses. We therefore posited that genes in Cluster 1, Cluster 2 and Cluster 4a did not contribute significantly to the defective recall response in *Tcf7*$^{\Delta Gzmb}$ CD8$^+$ T_{cm} cells.

Next, Tcf1 ChIP-seq on resting wild-type CD8$^+$ T_{cm} cells[28] identified 12,851 high-confidence Tcf1 binding sites. Stratifying with the DEG clusters indicated prevalent Tcf1 binding at promoter regions (defined as +/−3 kb sequence flanking transcription start site,

TSS) of genes in Cluster 2, Cluster 3 and Cluster 4a (Fig. 3e, middle column). For genes in Cluster 1 and Cluster 4b, Tcf1 binding sites were more frequently found at distal regions (gene body and its +/− 50 kb flanking sequence excluding promoters) (Fig. 3e, right columns). These data suggested that Tcf1 bound to key genes loci in resting CD8$^+$ T_{cm} cells and hence predetermined their transcriptional activation upon recall stimulation.

Tcf1 predetermines CD8$^+$ T_{cm} chromatin opening by recall

Wild-type CD8$^+$ T_{cm} cells expressed lower levels of Tcf1 than naïve CD8$^+$ T cells, and rapidly downregulated Tcf1 after 24-hr GP33 stimulation (Fig. 4a). Pretreatment of CD8$^+$ T_{cm} cells with a PI3-K inhibitor LY294002 or a calcineurin inhibitor Cyclosporin A substantially alleviated Tcf1 downregulation, whereas neither benzoxathiole nor selumetinib, which inhibits IKKβ and MEK respectively[29, 30], significantly prevented GP33-induced Tcf1 downregulation (Fig. 4b), suggesting PI3-K and calcineurin-NFAT were the dominant pathways that downmodulated Tcf1 expression in recall-stimulated CD8$^+$ T_{cm} cells.

ATAC-seq analysis before and after 24-hr stimulation with GP33 showed strong chromatin accessibility (ChrAcc) diversification between resting and stimulated states in both wild-type and *Tcf7*$^{\Delta Gzmb}$ CD8$^+$ T_{cm} cells (Extended Data Fig. 4a). Among the 42,605 ChrAcc sites detected, few sites showed differential ChrAcc between resting wild-type and *Tcf7*$^{\Delta Gzmb}$ CD8$^+$ T_{cm} cells (Fig. 4c); in contrast, GP33 stimulation caused robust ChrAcc increase at 17,763 sites, referred to as ‘recall-opened’ sites, and ChrAcc decrease at 1,484 sites (‘recall-closed’ sites) in wild-type CD8$^+$ T_{cm} cells (Fig. 4d). Analysis with genomic regions enrichment of annotations tool (GREAT)[31] showed that both recall-opened and recall-closed ChrAcc sites were enriched in “regulation of immune system process”, “T cell activation” and “cytokine receptor activity” (Fig. 4e, Extended Data Fig. 4b), indicating rapid activation of CD8$^+$ T_{cm} cells. The recall-opened ChrAcc sites were enriched for motifs of transcription factors downstream from the TCR (including AP-1, NF-κB and NFAT), and cytokine receptors (IRF and STAT), while the recall-closed ChrAcc sites were enriched with ETS, RUNX and Tcf/Lef motifs (Extended Data Fig. 4c,d). In fact, 986 (66%) of the 1,484 recall-closed sites overlapped with Tcf1 binding sites in resting wild-type CD8$^+$ T_{cm} cells (Fig. 4d), concordant with Tcf1 downregulation in recall-stimulated CD8$^+$ T_{cm} cells (Fig. 4a).

GP33 stimulation caused fewer ChrAcc changes in *Tcf7*$^{\Delta Gzmb}$ compared to wild-type CD8$^+$ T_{cm} cells, with 10,704 recall-opened and 986 recall-closed sites (Fig. 4f). 7,234 ChrAcc sites were opened in stimulated wild-type but not *Tcf7*$^{\Delta Gzmb}$ CD8$^+$ T_{cm} cells (Fig. 4g), and the ATAC-seq signals at these sites were higher in stimulated wild-type than stimulated *Tcf7*$^{\Delta Gzmb}$ CD8$^+$ T_{cm} cells, with the difference significantly greater than that between resting wild-type and resting *Tcf7*$^{\Delta Gzmb}$ CD8$^+$ T_{cm} cells (Fig. 4h). Among the 10,529 sites that were opened in both stimulated wild-type and stimulated *Tcf7*$^{\Delta Gzmb}$ CD8$^+$ T_{cm} cells, 1,277 sites had stronger ATAC-seq signals in stimulated wild-type than stimulated *Tcf7*$^{\Delta Gzmb}$ CD8$^+$ T_{cm} cells (Fig. 4h). The 7,234 and 1,277 sites (Fig. 4h) were collectively designated as ‘WT-prepotent’ ChrAcc sites, with the shared feature of showing stronger ATAC-seq signals in stimulated wild-type over stimulated *Tcf7*$^{\Delta Gzmb}$ CD8$^+$ T_{cm} cells.

Among the 8,511 WT-prepotent ChrAcc sites, 237 (2.8%) overlapped with Tcf1-binding sites in resting wild-type $CD8^+$ T_{cm} cells, and these $Tcf1^+$ ChrAcc sites were most enriched with Tcf/Lef (TCF7L2 and TCF7L1) and AP-1 motifs (FOSB and JUNB) (Fig. 4i); in contrast, all top ten motifs enriched at $Tcf1^-$ WT-prepotent ChrAcc sites were AP-1 motifs (Fig. 4i), suggesting a strong contribution of AP-1 factors to recall-opened ChrAcc sites. These observations suggested that Tcf1 predetermined the accessibility of most poised enhancers to recall-activated AP-1 and other factors in resting $CD8^+$ T_{cm} cells, without direct pre-occupancy.

Tcf1 integrates $CD8^+$ T_{cm} transcriptomic and ChrAcc changes

To integrate Tcf1-controlled molecular events, we focused on the 623 genes in Cluster 3 and Cluster 4a. Among these genes, Tcf1-binding sites were found in 364 promoters (58%) and in the distal regulatory regions of 468 genes (75%) in resting $CD8^+$ T_{cm} cells, with a substantial portion (44%) harboring Tcf1-binding sites in both promoter and distal regions (Fig. 5a, Supplementary Table 2). Additionally, 398 genes (64%) were associated with 634 WT-prepotent ChrAcc sites, which were mostly located in distal regions (Fig. 5b, Supplementary Table 3). Consistently, AP-1 motifs were more frequently found in distal regions of Cluster 3 and Cluster 4a genes compared to non-DEGs, but rarely observed at promoters (Fig. 5c). Although Tcf1-binding sites and WT-prepotent ChrAcc sites had distinct distribution patterns, 364 gene loci contained both (Fig. 5d). For example, the *Id3* locus was flanked by Tcf1-binding sites and WT-prepotent ChrAcc sites in its distal regions, and the *Ezh2* promoter was bound by Tcf1 and had an upstream WT-prepotent ChrAcc site (Fig. 5e). Additionally, genes encoding key glycolytic enzymes, such as *Gapdh*, *Pfkp*, *Pgk1* and *Pkm*, harbored Tcf1-binding sites in their promoters and had at least one WT-prepotent ChrAcc sites in their distal regions (Fig. 5f). Therefore, the WT-prepotent ChrAcc sites could function as poised enhancers in resting $CD8^+$ T_{cm} cells, and the co-enrichment with Tcf1-binding sites could facilitate their coordinated activation of key target genes in recall-stimulated $CD8^+$ T_{cm} cells.

Tcf1 mediates $CD8^+$ T_{cm} chromatin interactions

Because Tcf1 and Lef1 regulates 3D genome organization in naïve $CD8^+$ T cells[28, 32, 33], we next investigated if Tcf1 utilized its architectural role to coordinate recall responses of $CD8^+$ T_{cm} cells. We performed Hi-C in resting wild-type and $Tcf7^{\Delta Gzmb}$ $CD8^+$ T_{cm} cells, and generated data with good reproducibility between replicates despite low numbers of T_{cm} cells (Extended Data Fig. 5a). In wild-type $CD8^+$ T_{cm} cells, the density of Tcf1-binding peaks positively correlated with topologically associating domain (TAD) scores, which measured the level of intra-TAD chromatin interactions (ChrInt) (Fig. 6a). Using diffHiC[34], we identified 27,978 ChrInt pairs that showed diminished ChrInt strength in $Tcf7^{\Delta Gzmb}$ compared to wild-type $CD8^+$ T_{cm} cells. Among these, 3,934 ChrInt pairs harbored Tcf1-binding sites in at least one anchor, which were defined as “Tcf1-dependent ChrInt” and analyzed for their connection with target gene expression in $CD8^+$ T_{cm} cells. Because the current consensus is that long-range ChrInt mediate contact between promoters and distal enhancers (Fig. 6b), we required that one ChrInt anchor must overlap with a gene promoter. In resting $CD8^+$ T_{cm} cells, Tcf1-dependent ChrInt were highly enriched in Tcf1-activated genes in Cluster 4b compared to Tcf1-repressed Cluster 1 genes (Fig. 6c), as seen at the *Pld2*

locus (encoding phospholipase D2) (Fig. 6d). This observation suggested that Tcf1 engaged gene promoters with distal regulatory regions for positive regulation in resting $CD8^+$ T_{cm} cells. In addition, Tcf1-dependent ChrInt spanned target genes, with no overlap between ChrInt anchors and gene promoters (Fig. 6e). This type of 'gene-spanning' Tcf1-dependent ChrInt were also more enriched in Cluster 4b than Cluster 1 genes (Fig. 6f), as seen at the *Apobec2* locus (Fig. 6g). We posited that Tcf1-mediated chromatin contacts brought gene promoters and distal regulatory element(s) into spatial proximity for target gene regulation.

We next investigated the connection between Tcf1-dependent ChrInt and gene induction in recall-stimulated $CD8^+$ T_{cm} cells. Tcf1-dependent ChrInt were more enriched in genes in Cluster 3 and Cluster 4a than those induced independent of Tcf1 (Fig. 6h). Collectively, 386 Tcf1-dependent ChrInt pairs were associated with 247 genes in Cluster 3 and Cluster 4a (Supplementary Table 4), which encompassed key functions including cell cycle, DNA replication and glycolysis (Extended Data Fig. 5b). Additionally, these 247 genes were associated with promoter-engaging, gene-spanning or both types of Tcf1-dependent ChrInt (Fig. 6i). For example, the promoter of *Atp5l* (encoding ATP synthase subunit G) interacted with Tcf1-bound upstream regions in wild-type $CD8^+$ T_{cm} cells, and the ChrInc strength was diminished in *Tcf7*$^{\Delta Gzmb}$ $CD8^+$ T_{cm} cells (Fig. 6j). *Id3* was flanked by Tcf1-bound ChrInt anchors that showed diminished strength in *Tcf7*$^{\Delta Gzmb}$ compared to wild-type $CD8^+$ T_{cm} cells (Fig. 6k). Furthermore, WT-prepotent ChrAcc sites were more frequently observed in these 247 Cluster 3 and Cluster 4a genes associated with Tcf1-dependent ChrInt than the remainder genes in these clusters (Fig. 6l). These data suggested that Tcf1-mediated ChrInt provided an orderly architectural environment which brought the poised enhancers in spatial proximity with target genes in resting T_{cm} cells (Extended Data Fig. 5c), and thus facilitated activation of these elements and their associated target genes upon recall stimulation.

Tcf1 preprograms glycolysis induction in $CD8^+$ T_{cm} cells

To determine the functional importance of Tcf1-preprogrammed genes, we performed gene set enrichment analysis (GSEA) of the DEGs in GP33-stimulated wild-type and *Tcf7*$^{\Delta Gzmb}$ $CD8^+$ T_{cm} cells, and identified "KEGG_GLYCOLYSIS" as one of the most enriched gene sets (Fig. 7a). Glycolysis is catalyzed by 10 distinct enzymes which degrade glucose to lactate, fueling primary effector $CD8^+$ T cell differentiation[35, 36] (Fig. 7b). Genes encoding all 10 glycolytic enzymes (or at least one isozyme), from *Hk1* (hexokinase 1, which catalyzes glucose phosphorylation), to *Pkm2* (pyruvate kinase, which catalyzes pyruvate production), were found in Cluster 3 (Fig. 7c). In addition, Tcf1-binding sites were found in 7 gene promoters (*Hk1*, *Gpi1*, *Pfkl*, *Gapdh*, *Pgk1*, *Pgam1* and *Pkm2*), *Hk1* and *Pfkp* introns and upstream of *Eno3* (Fig. 5f, Extended Data Fig. 6a). Furthermore, 7 of the 9 Tcf1-bound glycolytic genes were associated with WT-prepotent ChrAcc sites, located upstream of *Hk1*, *Gpi1* and *Pfkp*, in *Pfkp* and *Pgk1* introns and downstream of *Hk1*, *Pfkl*, *Gapdh* and *Pkm2* (Fig. 5f, Extended Data Fig. 6a). These glycolysis-associated genes were not differentially expressed in resting wild-type and *Tcf7*$^{\Delta Gzmb}$ $CD8^+$ T_{cm} cells, but showed compromised induction and chromatin opening in stimulated *Tcf7*$^{\Delta Gzmb}$ compared to wild-type $CD8^+$ T_{cm} cells, suggesting that Tcf1 preprogramed induction of glycolytic genes in recall-stimulated $CD8^+$ T_{cm} cells.

To examine glycolysis *in vivo*, we transferred sorted CD45.2$^+$ wild-type or *Tcf7*$^{\Delta Gzmb}$ CD8$^+$ T$_{cm}$ cells into wild-type CD45.1 recipients followed by LCMV-Arm infection the next day. At 5 day p.i., secondary effector CD8$^+$ T cells were sorted and analyzed with Seahorse Extracellular Flux Analyzer to track extracellular acidification rate (ECAR) and oxygen consumption rate (OCR). Glycolysis and glycolytic capacity, as measured following addition of glucose and oligomycin (an inhibitor of ATP synthase) respectively, were diminished in *Tcf7*$^{\Delta Gzmb}$ compared to wild-type T$_{cm}$-derived effector CD8$^+$ T cells (Fig. 7d,e), albeit the glycolytic reserve, measured after 2-DG addition, were unaffected (Fig. 7d,e). In mitochondria stress tests, basal and maximal respiration, as measured before oligomycin and after treatment with FCCP (a reagent uncoupling oxygen consumption from ATP production), had a modest but consistent decrease in *Tcf7*$^{\Delta Gzmb}$ compared to wild-type T$_{cm}$-derived effector CD8$^+$ T cells (Fig. 7f,g), while spare respiratory capacity (SRC), measured after addition of retenone/actinomycin was unaffected (Fig. 7f,g). These data highlighted a requirement for Tcf1 to activate glycolysis in recall-stimulated CD8$^+$ T$_{cm}$ cells.

Tcf1 acts upstream of Id3 induction in CD8$^+$ T$_{cm}$ cells

GP33 stimulation of wild-type CD8$^+$ T$_{cm}$ cells for 24 hrs rapidly induced CD25 and CD69 in most cells, before the downregulation of CD62L and IL-7Rα (Extended Data Fig. 7a). CD25^{hi}CD69^{hi} CD8$^+$ T$_{cm}$ cells showed more robust Id3 induction than CD25^{int}CD69^{int} CD8$^+$ T cells (Extended Data Fig. 7b). In GP33-stimulated *Tcf7*$^{\Delta Gzmb}$ CD8$^+$ T$_{cm}$ cells, however, the ratio of CD25^{hi}CD69^{hi} to CD25^{int}CD69^{int} subsets was reversed, and Id3 induction was diminished in both subsets compared to their wild-type counterparts (Fig. 7h), suggesting that Tcf1 deficiency delayed activation of CD8$^+$ T$_{cm}$ cells and reduced the magnitude of gene induction upon recall stimulation.

To test whether the ectopic expression of Tcf1-preprogrammed genes could rectify the defective responses in recall-stimulated *Tcf7*$^{\Delta Gzmb}$ CD8$^+$ T$_{cm}$ cells, we cloned *Id3* or *Irf8* or a group of 4 glycolytic genes (*Aldoa*, *Gapdh*, *Pkm2* and *Ldha*; Gly4 herein) in bicistronic retroviruses that co-expressed mCherry or hNGFR (human nerve growth factor receptor), and then transduced each into bone marrow progenitors from wild-type or *Tcf7*$^{\Delta Gzmb}$ CD45.2 mice followed by transplantation into irradiated CD45.1 wild-type hosts (Extended Data Fig. 7c). In the resulting chimeric mice, donor-derived CD45.2$^+$mCherry$^+$ (hNGFR$^+$)CD8$^+$ T cells were mostly CD62L$^+$CD44$^{lo\text{-}med}$ (Extended Data Fig. 7d), demonstrating their suitability for assessing anti-viral responses. When naïve mCherry$^+$ (hNGFR$^+$) CD8$^+$ T cells were transferred into CD45.1 wild-type recipients followed by LCMV-Arm infection, the resulting CD8$^+$ T$_{cm}$ cells expressed the retrovirus-delivered genes at ≥30 day p.i (Fig. 8a, Extended Data Fig. 7e). As expected, fewer empty vector (*EV*)-mCherry$^+$CD8$^+$ T$_{cm}$ cells were generated from *Tcf7*$^{\Delta Gzmb}$ compared to wild-type donor cells, and forced expression of *Id3*, *Irf8* or Gly4 did not improve CD8$^+$ T$_{cm}$ cell formation compared to *Tcf7*$^{\Delta Gzmb}$ *EV*-mCherry$^+$CD8$^+$ T$_{cm}$ cells (Extended Data Fig. 7f), consistent with the observation that these genes did not depend on Tcf1 for basal transcription in resting CD8$^+$ T$_{cm}$ cells.

qRT-PCR analysis of sorted mCherry$^+$(hNGFR$^+$)CD8$^+$ T$_{cm}$ cells indicated that *Id3*, *Irf8* and Gly4 were similarly expressed in resting wild-type and *Tcf7*$^{\Delta Gzmb}$ *EV*-mCherry$^+$CD8$^+$ T$_{cm}$ cells, and were induced in GP33-stimulated wild-type *EV*-mCherry$^+$CD8$^+$ T$_{cm}$ cells, but less induced in GP33-stimulated *Tcf7*$^{\Delta Gzmb}$ *EV*-mCherry$^+$CD8$^+$ T$_{cm}$ cells (Fig. 8a,b). Ectopic expression of *Id3*, but not *Irf8*, almost fully restored the expression of *Pkm2* and partly improved *Gapdh* and *Ldha* induction in GP33-stimulated *Tcf7*$^{\Delta Gzmb}$ mCherry$^+$CD8$^+$ T$_{cm}$ cells (Fig. 8b), suggesting that Id3 induction contributed to activating glycolysis in recall-stimulated CD8$^+$ T$_{cm}$ cells.

Sorted CD45.2$^+$mCherry$^+$(hNGFR$^+$)CD8$^+$ T$_{cm}$ cells were then transferred into CD45.1 wild-type recipients followed by LCMV-Arm infection. At day 8 p.i., compared with wild-type, *Tcf7*$^{\Delta Gzmb}$ *EV*-mCherry$^+$CD8$^+$ T$_{cm}$ cells generated fewer secondary effector CD8$^+$ T cells, which was partially rescued by the ectopic expression of *Id3*, but not *Irf8* or Gly4 (Fig. 8c). Additionally, *Tcf7*$^{\Delta Gzmb}$ *Id3*-mCherry$^+$ secondary effector CD8$^+$ T cells had improved glycolysis and glycolytic capacity compared to *EV*-mCherry$^+$ counterparts (Fig. 8d,e). Gly4 expression only modestly improved glycolysis, but did not improve the glycolytic capacity of *Tcf7*$^{\Delta Gzmb}$ secondary effector CD8$^+$ T cells (Fig. 8d,e), consistent with a broad impact of Tcf1 deficiency at all glycolytic steps.

To substantiate the connection between Id3 and activation of glycolysis in CD8$^+$ T$_{cm}$ recall response, we transferred in vivo-primed, *EV*- or *Id3*-mCherry retrovirus-transduced CD45.2$^+$ wild-type and *Tcf7*$^{\Delta Gzmb}$ CD8$^+$ T cells into CD45.1 wild-type recipients, followed by LCMV-Arm infection (Extended Data Fig. 7g). At ≥30 day p.i., the number of wild-type or *Tcf7*$^{\Delta Gzmb}$ *Id3*-mCherry$^+$CD8$^+$ T$_{cm}$ cells was higher than their *EV*-mCherry$^+$ counterparts (Extended Data Fig. 7h). When transferred into *Tcra*$^{-/-}$ mice, wild-type or *Tcf7*$^{\Delta Gzmb}$ *Id3*-mCherry$^+$CD8$^+$ T$_{cm}$ cells generated higher numbers of secondary effector CD8$^+$ T cells (Fig. 8f) and had improved glycolysis and glycolytic capacity (Fig. 8g, h) than the corresponding *EV*-mCherry$^+$CD8$^+$ T$_{cm}$ cells at day 5 post-LM-GP33 infection. In addition, the recipients of wild-type or *Tcf7*$^{\Delta Gzmb}$ *Id3*-mCherry$^+$CD8$^+$ T$_{cm}$ cells had reduced bacterial burden in the liver than those of corresponding *EV*-mCherry$^+$CD8$^+$ T$_{cm}$ cells (Fig. 8i). These observations indicated that ectopic expression of *Id3* boosted recall responses in Tcf1-sufficient and Tcf1-deficient CD8$^+$ T$_{cm}$ cells, partly through enhancing glycolysis activation.

Discussion

Here we showed a unique requirement for Tcf1 in pre-programming the differentiation of CD8$^+$ T$_{cm}$ cells into secondary effector CD8$^+$ T cells. Tcf1 was essential for recall-stimulated CD8$^+$ T$_{cm}$ cells to mobilize its downstream transcriptional regulators and glycolysis, in order to meet the bioenergetic needs required for CD8$^+$ T cell effector expansion. These findings highlighted the interconnectivity between self-renewal and differentiation in CD8$^+$ T$_{cm}$ cells, with Tcf1 as a central modulator of both processes[6, 37].

The differentiation of naïve CD8$^+$ T cells to cytotoxic effectors is accompanied by a metabolic switch from catabolic oxidative phosphorylation to aerobic glycolysis[35, 36], while memory CD8$^+$ T cells revert to catabolic metabolism, with increased mitochondrial mass

and greater mitochondrial spare respiratory capacity[38]. We found that $CD8^+$ T_{cm} cells rapidly induced glycolytic genes within 24 hrs upon recall stimulation to enhance the energy supply for expansion of secondary effector $CD8^+$ T cells. This process required Tcf1 in $CD8^+$ T_{cm} cells at resting state and Tcf1-dependent Id3 induction during the recall response. Ectopic *Id3* expression not only boosted the glycolytic capacity of Tcf1-sufficient $CD8^+$ T_{cm} cells, but also partly restored induction of glycolytic genes and secondary expansion of Tcf1-deficient $CD8^+$ T_{cm} cells. This established a direct link between Id3 and glycolysis activation in $CD8^+$ T_{cm} cells. Because recall-stimulated $CD8^+$ T_{cm} cells downregulated Tcf1 but upregulated Id3, our findings suggested a functional relay among transcriptional regulators to support the robust proliferation of $CD8^+$ T_{cm} cells during recall responses.

Tcf1 downregulation is necessary for effective expansion of effector $CD8^+$ T cells during the primary responses[20, 39]. Similarly, $CD8^+$ T_{cm} cells rapidly downregulated Tcf1 upon re-stimulation by cognate antigen. It seemed counter-intuitive that a transcription factor that is downregulated/silenced in recall-stimulated $CD8^+$ T_{cm} cells could control their proliferative potential. Our molecular analyses demonstrated that Tcf1 deficiency had a broad and profound impact on the magnitude of expression induction and chromatin opening in genes controlling cell cycle progression and cellular energy production in recall-stimulated $CD8^+$ T_{cm} cells, while most of these defects were not observed in resting Tcf1-deficient $CD8^+$ T_{cm} cells. These observations highlight the importance of a ‘stress test’ to reveal the mechanistic and biological roles of key regulators in memory T cells. Our findings suggested that Tcf1 critically regulated the preparedness of resting $CD8^+$ T_{cm} cells to respond to secondary challenges, and we propose the concept of “preprogramming” to describe this key function of Tcf1 in $CD8^+$ T_{cm} cells.

Global mapping of transcription factor occupancy has revealed that most factors bind to many more gene loci than the number of genes regulated in a specific cell state. The “inconsequential” binding by transcription factors has been puzzling, and is considered to serve a ‘community’ role in large protein complexes. The preprogramming function by Tcf1 offers a logical alternative explanation for its broad occupancy in $CD8^+$ T_{cm} cell genome. Tcf1 bound extensively to promoters in Cluster 3 genes in resting $CD8^+$ T_{cm} cells without apparently affecting their expression, while the biological impact of these Tcf1-binding events became detectable only when $CD8^+$ T_{cm} cells differentiated into secondary effector cells in response to recall stimulation. About half of the recall-opened ChrAcc sites in $CD8^+$ T_{cm} cells showed inadequate chromatin opening in the absence of Tcf1; however, only a small fraction of these sites were pre-occupied by Tcf1 in resting $CD8^+$ T_{cm} cells, indicating that these poised enhancers did not require Tcf1 as a placeholder for transcription factors mobilized by TCR ligation. Hi-C analysis indicated that the recall-induced genes were associated with Tcf1-dependent chromatin interactions, which encompassed Tcf1-dependent, recall-opened ChrAcc sites. The Tcf1-dependent chromatin interactions may create an orderly architectural environment so that the poised enhancers in distal regions are brought into spatial proximity with recall-induced gene promoters, inducing a ‘preprogrammed’, activation-ready state. In this context, the disruption of chromatin interaction due to loss of Tcf1 may not affect the expression of associated genes in resting $CD8^+$ T_{cm} cells, but impact how these genes respond to incoming TCR signals. Our integrative analyses highlight an essential requirement for Tcf1’s structural role in 3D

genome organization in CD8$^+$ T_{cm} cells to preprogram their responsiveness to secondary challenge.

METHODS

Mice.

C57BL/6J (B6), B6.SJL and Rosa26^{GFP} mice were from the Jackson Laboratory. *Tcf7*$^{fl/fl}$, *Lef1*$^{fl/fl}$ and *Gzmb*-Cre transgenic mice were described[40, 41]. They were either generated on C57BL/6 background or backcrossed to C57BL/6 for ≥10 generations. All compound mouse strains used in this work were from in-house breeding at animal care facilities of the University of Iowa and Hackensack University Medical Center. The mice were housed at 18–23°C with 40–60% humidity, with 12 light/12 dark cycles. All mice analyzed were 6–12 weeks of age, and both sexes are used without randomization or blinding. All mouse experiments were performed under protocols approved by the Institutional Animal Use and Care Committees of the University of Iowa and that of Hackensack University Medical Center.

Adoptive transfer and acute infection.

To elicit a primary response, naïve P14 CD8$^+$ T cells, isolated from the lymph nodes (LNs) of P14 wild-type, *Tcf7*$^{\Delta Gzmb}$, *Tcf7*$^{\Delta Gzmb}$*Lef1*$^{\Delta Gzmb}$ mice, were adoptively transferred into B6.SJL recipients (2×10^4 cells/recipient). On the following day, the recipients were intraperitoneally (*i.p*) infected with 2 × 10^5 PFU of LCMV-Arm. For a recall response, CD62L$^-$ effector or CD62L$^+$ central memory P14 CD8$^+$ T cells were sort-purified from the primary recipients at 30–35 *dpi*, and then adoptively transferred into another cohort of naïve wild-type B6.SJL (500–1,000 cells/recipient) or *Tcra*$^{-/-}$ mice (2,000 cells/recipient) followed by *i.p*. infection with LCMV-Arm (2×10^5 PFU) or *i.v*. infection with LM-GP33 (2×10^6 CFU), respectively. For characterization of CD8$^+$ T_{cm} cells in early cell divisions upon secondary challenge, sorted T_{cm} cells were labeled with CTV and adoptively transferred into wild-type B6.SJL recipients (1×10^5 cells/recipient). The recipients were then *i.v*. infected with LCMV-Arm, and 60 hrs later, the activated T_{cm} cells were analyzed in the recipient spleens.

Flow cytometry.

Single-cell suspensions from the spleen and lymph nodes (LNs) were generated after mashing tissue through 70 μm cell strainer, and the cells were surface-, intracellularly or intranuclearly stained following standard protocols[42]. The fluorochrome-conjugated antibodies, including anti-CD8 (53–6.7), anti-TCRβ (H57–597), anti-CD44 (IM7), and anti-CD62L (MEL-14), anti-CD45.2 (104), anti-KLRG1 (2F1), anti-IL-7Ra (A7R34), anti-Granzyme B (GB12), anti-IFN-g (XMG1.2), anti-TNF (MP6-XT22), anti-IL-2 (JES6–5H4), anti-hNGFR (ME20.4), were from eBiosciences, ThermoFisher Scientific. Anti-Tcf1 (C63D9) was from Cell Signaling Technology, and anti-Id3 (S30–778) was from BD Biosciences. For intranuclear detection of Id3 or Tcf1, surface-stained cells were fixed and permeabilized with the Foxp3/Transcription Factor Staining Buffer Set (eBiosciences, ThermoFisher Scientific), followed by incubation with corresponding fluorochrome-conjugated antibodies. For cytokine staining, the cells were stimulated with GP33 (200 nM)

in the presence of the protein transport inhibitor Brefeldin A for 5 hrs at 37°C, followed by standard intracellular staining. Cell sorting was performed on FACSAria (BD Biosciences). Data were collected on Fortessa LSR or FACSCelesta flow cytometers (BD Biosciences) and were analyzed with FlowJo software v10.7.1 (TreeStar).

Ex vivo analysis of CD8$^+$ T_{cm} cells.

Wild-type or *Tcf7*$^{\Delta Gzmb}$ CD62L$^+$CD8$^+$ T_{cm} cells were sort-purified from the primary recipients at 30–35 *dpi* and seeded onto flat bottom 96-well plate at 1×10^5 cells/well and incubated with GP33 peptide (200 nM) for 24 hrs, with dead cells removed using a Dead Cell Removal Kit (Miltenyi Biotec). The cells were used as GP33-stimulated CD8$^+$ T_{cm} cells for RNA-seq and ATAC-seq analyses. For detection of IFN-γ production, Brefeldin A was added during the last 5 hrs of incubation. For mapping pathways leading to Tcf1 downregulation, Wild-type CD8$^+$ T_{cm} cells were enriched with EasySep PE Positive Selection Kit (StemCell Technologies) after staining with CD62L-PE, and the cells were pre-incubated with pharmacological inhibitors or DMSO carrier for 30 min followed by 24-hr coculture with GP33. Benzoxathiole (Abcam, Cat. No. ab145954), Cyclosporin A, LY294002, and Selumetinib (Millipore-Sigma, Cat. No. 30024, 440202, and ADV465749271, respectively) were used at the final concentrations of 10 μM, 140 nM, 14 μM and 70 nM, which were equivalent to 10× their respective reported IC50 (Ref.[29, 30]).

Retroviral transduction and assessment of *in vivo* rescue effect.

Id3 or *Irf8* cDNA was cloned into an mCherry-expressing retroviral vector (mCherry-RV, from Addgene). For genes encoding glycolytic enzymes, coding sequences of *Gapdh* and *Aldoa* cDNAs were linked with 2A peptide cDNA sequence and cloned into mCherry-RV, those of *Pkm2* and *Ldha* cDNAs were linked with 2A peptide cDNA and were cloned into hNGFR-expressing retroviral vector (hNGFR-RV, Addgene). Selection of these four glycolytic genes was based on the more pronounced defective induction in GP33-stimulated *Tcf7*$^{\Delta Gzmb}$ CD8$^+$ T_{cm} cells and/or lack of compensatory isozymes during the glycolytic process. The retrovirus was packaged in 293T cells as previously described[43].

For the primary ‘rescue’ approach as outlined in Extended Data Fig. 7c, bone marrow (BM) cells from CD45.2$^+$ WT or *Tcf7*$^{\Delta Gzmb}$ P14-TCR transgenic mice were depleted of lineage-positive cells to enrich hematopoietic stem/progenitor cells, and the Lin$^-$ BM cells were infected with mCherry-expressing RV alone, or co-infected with *Gapdh-Aldoa*-mCherry and *Pkm2-Ldha*-hNGFR RVs (so as to achieve ectopic expression of 4 glycolytic genes, called Gly4). The RV-infected BM cells were then transplanted into irradiated CD45.1$^+$ recipients to establish BM chimeras. Eight weeks later, mCherry$^+$ or mCherry$^+$hNGFR$^+$ naïve P14 CD8$^+$ T cells were sort-purified from LNs of the BM chimeras and used for adoptive transfer and infection studies to generate CD8$^+$ T_{cm} cells as detailed above. The resulting CD8$^+$ T_{cm} cells, at resting state or after GP33 stimulation, were collected for RNA extraction and reverse transcription, followed by quantitative PCR to validate ectopic expression of genes of interests. Primers used for RT-PCR were as the following: *Hprt1*:5’-gcgtcgtgattagcgatgatg and 5’-ctcgagcaagtctttcagtcc; *Id3:* 5’-ttagccaggtggaaatcctg and 5’-agtgagctcagctgtctgga; *Irf8:* 5’-ggatatgccgcctatgacaca and 5’-catccggcccatacaacttag; *Aldoa:* 5’-gctgtcactggggtcacttt and 5’-agtcaaggcccatggcttc; *Gapdh:* 5’-aactttggcattgtggaagg

and 5’-acacattgggggtaggaaca; *Pkm2:* 5’-ctgcaggtgaaggagaaagg and 5’-agatgcaaacaccatgtcca; *Ldha:* 5’-ccgttacctgatgggagaga and 5’-gtaggcactgtccaccacct.

For the alternative ‘rescue’ approach as outlined in Extended Data Fig. 7g, wild-type or *Tcf7*$^{\Delta Gzmb}$ P14-TCR transgenic mice were *i.v.* infected with 2 × 10^6 PFU of LCMV-Arm to prime the P14 CD8$^+$ T cells *in vivo*. One day later, the splenocytes were infected with empty vector (*EV*)- or *Id3*-mCherry retrovirus by spinofection (at 2500 rpm, 37°C for 90 min) in the presence of anti-CD28 (clone 37.51, eBiosciences), human IL-2 (100 U/ml) and GP33 peptide (200 nM), and then cultured overnight. The spinofection was repeated the next day, and the cells were cultured in fresh RP10 media in the absence of anti-CD28, IL-2 and GP33 peptide for 20–24 hrs. The retrovirally infected P14 CD8$^+$ T cells (containing 1×10^4 mCherry$^+$ cells together with their mCherry$^-$ counterparts) were adoptively transferred into B6.SJL recipients and then *i.p.* infected with 2×10^5 PFU of LCMV-Arm the following day. On ≥ 25 *dpi*, the mCherry$^+$CD62L$^+$ CD8$^+$ T_{cm} cells were enumerated and sort-purified for adoptive transfer into *Tcra*$^{-/-}$ recipients for *in vivo* characterization.

Metabolism assays.

CD8$^+$ T_{cm} cells generated from the primary response were sorted and adoptively transferred into naive wild-type B6.SJL recipients followed by LCMV-Arm infection, or into *Tcra*$^{-/-}$ recipients followed by LM-GP33 infection. Five days later, CD45.2$^+$ P14 secondary effector KLRG1$^+$CD8$^+$ T cells were sort-purified and were seeded onto a 96-well plate at 1–2 ×10^5 cells per well. ECAR and OCR were measured using the XF-96 Extracellular Flux Analyzer (Seahorse Bioscience). The ECAR measurements were performed under basal conditions in Seahorse XF medium supplemented with 2 mM L-glutamine, and in response to 10 mM glucose, 1 μM oligomycin, and 50 mM 2-Deoxy-D-glucose. The OCR measurements were performed under basal conditions in Seahorse XF medium supplemented with 2 mM L-glutamine, 25 mM glucose, and 1 mM sodium pyruvate, and in response to 1 μM oligomycin, 1.5 μM fluorocarbonyl cyanide phenylhydrazone (FCCP), and 0.5 μM rotenone + 1 μM antimycin A.

RNA-seq and data analysis.

Wild-type or *Tcf7*$^{\Delta Gzmb}$ CD8$^+$ T_{cm} cells, at resting state or after GP33 stimulation, were collected in two biological replicates for each cell type/state. cDNA synthesis, amplification and library construction were performed using SMARTer Ultra Low Input RNA Kit (Clontech, Takara Bio), as previously described[42]. The libraries were sequenced on Illumina’s HiSeq4000 in paired read mode with the read length of 150 nucleotides at the Admera Health. Sequencing data in fastq format were generated using CASAVA 1.8.2 processing pipeline from Illumina. The RNA-seq data are deposited at the GEO (accession number GSE177064).

Sequenced reads were first trimmed by 30 bp from both ends to remove the low-quality bases. The trimmed paired-end reads were then mapped to the mouse genome mm10 using hisat2 (v2.1.0)[44], and only the pairs with mapping quality (MAPQ) ≥ 30 and both ends mapped to the same chromosome were retained. Expression index (RPKM, reads per kilobase of transcript per million mapped reads) was generated for each gene in each

replicate using StringTie[45] (v1.3.4) based on the mm10 Refseq annotation. Differentially expressed genes (DEGs) were identified using DESeq2 (v1.12.4)[46] with default cutoff (adjusted p-value < 0.1). The fold change of DEGs was estimated using the apeglm method[47] for downstream analyses. To further reduce the false positive rate of DEGs, two additional criteria were applied to DEG detection: 1) apeglm-estimated fold change ≥ 1.5, and 2) RPKM in higher expression condition ≥ 1. Genes showing significant differential expression between wild-type or *Tcf7*$^{\Delta Gzmb}$ CD8$^+$ T$_{cm}$ cells in either resting or GP33-stimulated condition were combined as Tcf1-modulated genes. Unsupervised K-means clustering (k=7) was performed on the Tcf1-modulated genes based on their apeglm-estimated log2 fold changes in different comparisons (resting *Tcf7*$^{\Delta Gzmb}$ CD8$^+$ T$_{cm}$ cells *vs.* resting wild-type CD8$^+$ T$_{cm}$ cells, GP33-stimulated wild-type CD8$^+$ T$_{cm}$ cells *vs.* resting wild-type CD8$^+$ T$_{cm}$ cells, and GP33-stimulated *Tcf7*$^{\Delta Gzmb}$ CD8$^+$ T$_{cm}$ cells *vs.* GP33-stimulated wild-type CD8$^+$ T$_{cm}$ cells). The log2 fold changes for each comparison were scaled (divided by the standard deviation of log2 fold changes of all the included DEGs in the corresponding comparisons) before the K-means clustering. Functional annotation of DEGs was performed using DAVID Bioinformatics Resources 6.8.

In enrichment analysis of Tcf1-dependent chromatin interactions (Fig. 6h), a list of 1,788 Tcf1-independent, recall-induced genes was extracted as a negative control. These genes were identified as having significant higher expression in GP33-stimulated wild-type CD8$^+$ T$_{cm}$ cells than resting wild-type CD8$^+$ T$_{cm}$ cells but exhibiting little difference (≤1.2-fold changes) between GP33-stimulated *Tcf7*$^{\Delta Gzmb}$ and GP33-stimulated wild-type CD8$^+$ T$_{cm}$ cells.

ATAC-seq and data analysis.

Wild-type or *Tcf7*$^{\Delta Gzmb}$ CD8$^+$ T$_{cm}$ cells, at resting state or after GP33 stimulation, were purified as above. Two biological replicates for each cell type, and 50,000 cells for each replicate were used to prepare ATAC-seq libraries as previously described[42]. Briefly, the sorted cells were treated in lysis buffer for 3 min on ice, and the extracted nuclei were resuspended in transposition mix containing 2.5 μl Transposase (Illumina) and incubated at 37°C for 30 min. The products were purified with MinElute Reaction Cleanup Kit (Qiagen), and then amplified by PCR for 12 cycles with barcoded Nextera primers (Illumina). DNA fragments in the range of 150–1,000 bp were recovered from 2% E-Gel EX Agarose Gels (Invitrogen, ThermoFisher Scientific). The libraries were quantified using a KAPA Library Quantification kit and sequenced on Illumina HiSeq4000 in paired read mode with the read length of 150 nucleotides at the Admera Health. The ATAC-seq data were deposited in the GEO (accession number GSE177064).

The ATAC-seq reads were first mapped to the mouse genome mm10 with Bowtie2 (v2.3.5, paired-end mode, with additional parameters: −X 2000, −3 115)[48], and the paired-end reads mapped to unique genomic locations with MAPQ ≥ 30 and both ends mapped to the same chromosome were retained. ATAC-seq peaks for each cell type/state were called separately with MACS2 (v2.1.2, paired-end mode, with cutoff of q<0.01)[49]. The peaks identified from all cell types/states were then merged as the potential ChrAcc region candidates. ATAC-seq

peaks from different cell types/states and Tcf1 peaks were mapped to the merged peak set for all downstream analyses.

Because of a profound impact of TCR stimulation on ChrAcc diversification in $CD8^+$ T_{cm} cells compared with their resting state, a linear regression-based normalization strategy was designed so as to compare ATAC-seq signal changes more accurately among different cell types/states. This strategy was based on the assumption that actively transcribed genes with non-differential expression status among all cell types/states should have similar chromatin accessibility levels at their transcription start sites (TSSs) and proximal flanking regions. By requiring RPKM≥1 in both replicates in resting Wild-type $CD8^+$ T_{cm} cells and non-differential expression among any pairwise comparisons among the four cell types/states, 3,569 genes were extracted and used as a control gene set. The average ATAC-seq signals at the ± 1 kb regions flanking the TSSs of the control genes were obtained from both replicates of each cell type/state. To facilitate simultaneous comparison among multiple cell types/states in the univariate linear regression model, ATAC-seq signals of the control genes in resting wild-type $CD8^+$ T_{cm} cells were set as dependent variable (y), and those in other cell types/states as independent variable (x). The coefficient of the regression model was then applied to the genome-wide ATAC-seq signals in all other cell types/states, and the normalized ATAC-seq signals were used for downstream analyses.

DESeq2 (v1.12.4, Ref.[49]) was DESeq2 (v1.12.4)[46] was then applied to the normalized ATAC-seq signals to identify differential chromatin accessible (Diff ChrAcc) sites among different cell types/states. The merged ATAC-seq peaks from all cell types/states were used as the potential peak regions, and stringent cutoffs (adjusted p-value < 1e–5 and fold change ≥ 2) were applied to identify peaks showing Diff ChrAcc. The fold changes of Diff ChrAcc sites were estimated using apeglm[47].

Motif analysis.

For DNA sequence motif analysis of Diff ChrAcc sites between resting and GP33-stimulated wild-type $CD8^+$ T_{cm} cells (Extended Data Fig. 4c,d), HOMER (v4.11) motif analysis[50] was performed with default parameters. The top motifs were extracted with the corresponding statistics (p-value and percentage of targets). For functional annotation of Diff ChrAcc sites, the Genomic Regions Enrichment of Annotations Tool (GREAT, v.4.0.4) was used with default settings[31].

For analysis of motif enrichment at the WT-prepotent ChrAcc sites (Fig. 4i), a list of stable (*i.e.*, non-differential) ChrAcc sites was extracted as background. The stable ChrAcc sites were defined as sites with moderate average ATAC-seq signals (mean ≥ 1) and low variance (coefficient of variation ≤ 0.2) across samples from all 4 cell types/states, where the coefficient of variation was the ratio between the standard deviation and the mean of the normalized ATAC-seq signals. For each transcription factor (TF) motif i with motif in HOCOMOCO database[51], the genome-wide motif sites were identified by scanning the mouse reference genome (mm10) using FIMO (v4.12.0, p<1e–5)[52]. The likelihood of finding a motif site in $Tcf1^+$ or $Tcf1^-$ WT-prepotent sites was then compared with that in the stable ChrAcc sites. The likelihood ratio Λ_i is defined as:

$$\Lambda_i = \frac{\mathscr{L}_i^{prepotent}}{\mathscr{L}_i^{stable}}$$

where $\mathscr{L}_i^{prepotent}$ represents the percentage of WT-prepotent sites that overlap with motif sites of TF *i*, and $\mathscr{L}_i^{stable}$ represents the percentage of stable ChrAcc sites that overlap with motif sites of TF *i*. TFs with positive log likelihood ratio were deemed as 'enriched', while those with negative log likelihood ratio were deemed as 'depleted' in WT-prepotent sites compared with stable ChrAcc sites. Also included in the analysis were our previously published CBF ChIP-Seq peaks in naïve and effector $CD8^+$ T cells (GSM2471915 and GSM2471917, respectively)[43]. CBF ChIP-seq peaks were identified using the same method as described in the Tcf1 ChIP-seq data analysis section below.

For motifs with highest enrichment in the $Tcf1^-$ WT-prepotent ChrAcc sites, we also analyzed their enrichment in the regulatory regions of Tcf1-dependent, recall-induced Cluster 3 and Cluster 4a genes, using non-DEGs as control. Specifically, the percentages of each group of genes that harbored WT-prepotent ChrAcc site(s) with the motif in their promoters or distal regulatory regions were calculated separately. The significance of the relative enrichment of the motif between Clusters 3 and Cluster 4a genes and non-DEGs was assessed using the Fisher's exact test.

Tcf1 ChIP-seq in $CD8^+$ T_{cm} cells and data analysis.

Recombinant full-length Tcf1 protein was purified and used to immunize rabbits to obtain Tcf1 antisera, so as to increase the probability of capturing exposed Tcf1 epitopes especially in large protein complexes. Wild-type $CD8^+$ T_{cm} cells were sort-purified from primary recipients on 60 *dpi*, and naïve $CD8^+$ T cells from CD4-Cre^+ $Tcf7^{FL/FL}$ mice were used as a negative control. The sorted cells were fixed and lysed as detailed previously[28]. The nuclei were sonicated with a Q125 sonicator equipped with an 1/8-inch diameter probe (QSonica) at 20% input amplitude, at 20-second duration for eight times, and the chromatin fragments were immunoprecipitated with the anti-Tcf1 antiserum, followed by proper washing and library construction as previously documented[28]. The libraries were sequenced on HiSeq2000 in paired read mode with the read length of 150 nucleotides. The Tcf1 ChIP-seq data are deposited at the GEO (accession number GSE177064).

Tcf1 ChIP-seq reads were mapped to the mouse genome mm10 with Bowtie2 (v2.3.5, paired-end mode, with additional parameters: −X 2000, −3 115)[48], and the paired-end reads mapped to unique genomic locations with MAPQ ≥ 30 and both ends mapped to the same chromosome were retained. Genome-wide Tcf1 binding sites were identified with MACS14 (Ref.[49], with parameters p-value < 1e–5, --nomodel, --shiftsize 73) using the high-quality reads. The MACS-identified peaks with ≥ 5-fold enrichment over the control were retained as high-confidence Tcf1 binding sites. The genome-wide signals of Tcf1 ChIP-seq data were normalized by sequencing depth for unbiased visualization.

Association of Diff ChrAcc sites or Tcf1 binding sites to genes.

For assignment of Diff ChrAcc sites or Tcf1 binding sites to their target genes, a site that appears in a gene body and its +/−50 kb flanking region of the target gene was considered to be associated with that gene. A site located within +/− 3 kb from the TSS was designated as a promoter-associated site. A site located within gene body +/− 50 kb flanking region and outside of TSS +/−3 kb was assigned as a distal site. Note that one ChrAcc site could be associated with more than one unique Refseq gene.

Hi-C and data analysis.

Hi-C was performed using the three enzyme Hi-C (3e Hi-C) approach as previously described[28, 53]. In brief, wild-type or *Tcf7*$^{\Delta Gzmb}$ CD8$^+$ T_{cm} cells at the resting state were sort-purified as above (each in two replicates, 5×10^5 cells/replicate) and cross-linked with 1% formaldehyde for 10 minutes at 25°C. The crosslinked cells were lysed in 10 ml lysis buffer (10 mM Tris-HCl pH 8.0, 10 mM NaCl, 0.2% NP-40) supplemented with protease inhibitor cocktail (Millipore/Sigma) at 4°C for 1 hr. The nuclei were collected and treated with 400 μl 1×CutSmart buffer (NEB) containing 0.1% SDS at 65°C for 10 minutes, and Triton X-100 was added to a final concentration of 1% to quench SDS. The resulting chromatin was then digested with three restriction enzymes, CviQ I, CviA II, and Bfa I (NEB), at 20 units each at 37°C for 20 minutes. The reaction was stopped by washing with 600 μl wash buffer (10 mM NaCl, 1 mM EDTA, 0.1% Triton X-100) two times. The DNA ends were blunted and labeled with biotin by Klenow enzyme in the presence of dCTP, dGTP, dTTP, biotin-14-dATP, followed by ligation using T4 DNA ligase. After reverse crosslinking, DNA was fragmented by sonication with a Covaris S2 ultrasonicator. The DNA fragments were then end-repaired, and the biotinylated DNA fragments were captured using Dynabeads MyOne Streptavidin C1 beads (Invitrogen, Thermo Fisher Scientific). The DNA on beads was ligated to the Illumina Paired End Adaptors and amplified with PCR for library construction. DNA fragments of 300–700 bp were purified from 2% E-gel and sequenced on HiSeq4000 in paired read mode with the read length of 150 nucleotides. The Hi-C data were deposited at the GEO (accession number GSE177064).

Hi-C data (2 replicates each for wild-type or *Tcf7*$^{\Delta Gzmb}$ CD8$^+$ T_{cm} cells) were processed with the distiller-nf pipeline (v0.3.3, with default parameters)[53] onto reference genome mm10 and the resulting Hi-C raw count .cool files with 10-kb resolution were then processed into the sparse contact matrices with cooler (v0.8.11)[54]. Raw reads of the 2 replicates in each condition were pooled for identification of topologically associating domains (TADs) and 3D genome visualization. TADs were identified with the Arrowhead algorithm from Juicer v1.21.01[55] using the medium resolution maps (*i.e.*, m: 2000; resolution: 10kb; normalization: KR). The TAD score is defined as the ratio of the total number of intra-TAD read pairs divided by the total number of read pairs with at least one anchor overlapping with the TAD.

The raw-count contact matrices were subjected to distance normalization[56] as follows. For a matrix element M_{ij} with $|i-j| = d$, we counted the number of elements N_d with the same distance d in the same chromosome $N_d = \Sigma_{i,|i-j|=d} 1$. The average interaction of distance d on the same chromosome was $S_d = \Sigma_{i,|i-j|=d} M_{ij}/N_d$. The normalized matrix element

was defined as $\widehat{M}_{ij} = M_{ij}/S_d$. For distance-normalized contact matrices in each replicate, the respective row sum of the contact matrix elements (excluding the diagonal element) was calculated. Scatter plots of the resulting data were used to calculate the Pearson correlation of the replicates. The distance-normalized contact matrices were converted into .hic files using Juicer tools pre (v1.21.01) for visualization in WashU Epigenome Browser.

To identify differential chromatin interactions between wild-type or *Tcf7*$^{\Delta Gzmb}$ CD8$^+$ T_{cm} cells, diffHic (v4.1)[34] was applied to the replicates of Hi-C raw count data. In the diffHic analysis, interactions with the overall Negative Binomial mean across all samples no less than 3 were retained for differential chromatin interaction analysis using quasi-likelihood F-test. Significant differential interactions were identified with fold change ≥1.5 and *p*-value <0.05.

Statistical analysis.

For comparison between two experimental groups, Student's *t*-test was used. For multiple group comparisons, one way ANOVA was used to first determine whether any of the differences between the means are statistically significant, followed by 1) unpaired Student's *t*-test to determine the statistical significance for a specific pair, or 2) post hoc Tukey's multiple comparisons test to more stringently determine the statistical significance of differences between all possible pairs. Wilcoxon rank sum test (paired, one-sided) was used to compare the ATAC-seq signals in different cell types/states at target ChrAcc sites.

Extended Data

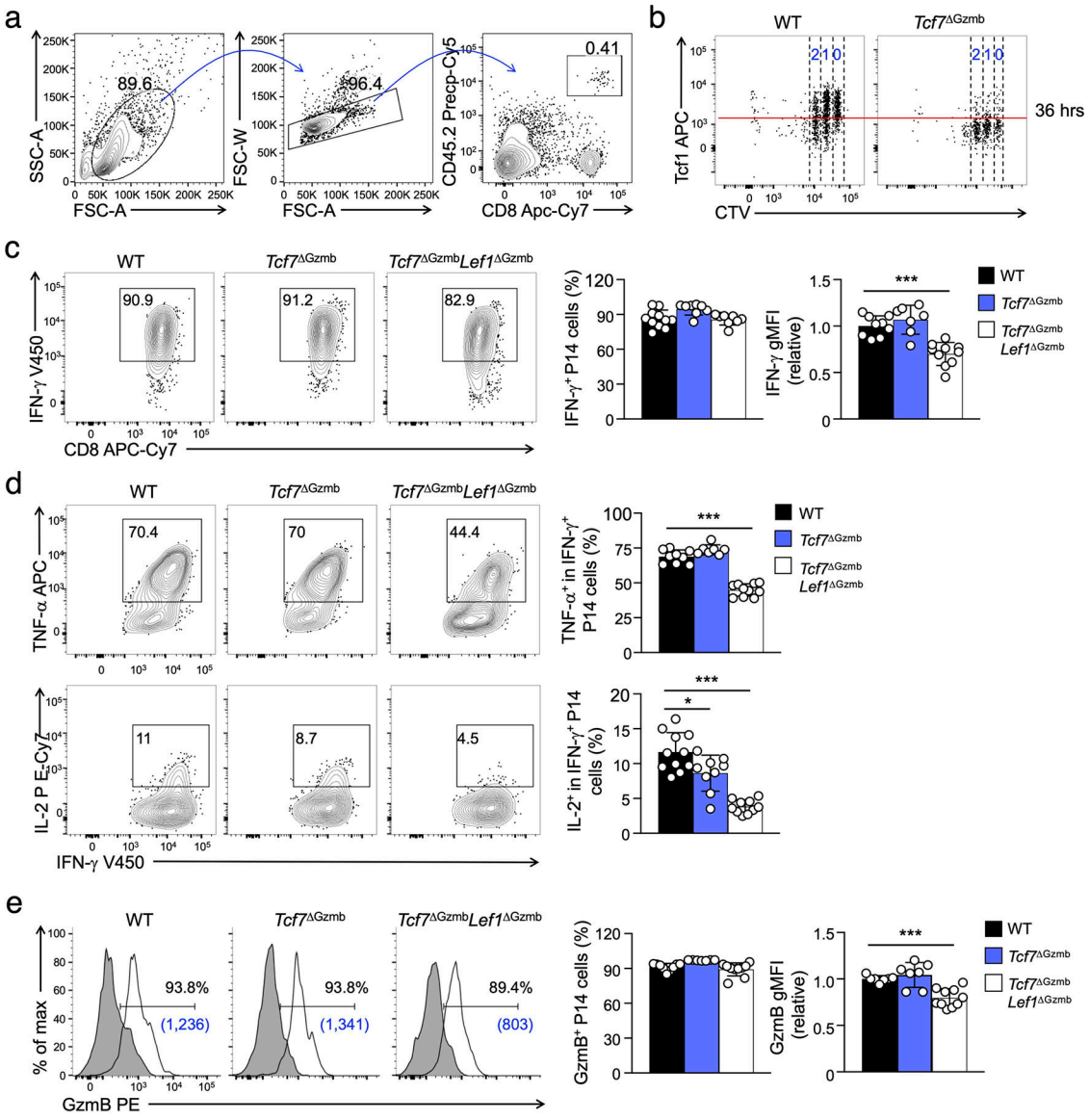

Extended Data Fig. 1. Double deletion of Tcf1 and Lef1 diminished expression of cytotoxic effector molecules during primary CD8$^+$ T cell responses.

a. Gating stratey to identify CD45.2$^+$ donor-derived P14 CD8$^+$ T cells in CD45.1$^+$ wild-type recipients.

b. Validating early deletion of Tcf1 protein by *Gzmb*-Cre by intracellular stating at 36 hrs after willd-type (WT) or *Tcf7*$^{\Delta Gzmb}$ P14 CD8$^+$ T cells were labeled with cell-trace violet (CTV) and adoptively transferred into CD45.1$^+$ recipients followed by *i.v.* infection with LCMV-Arm the next day. Dot plots are representative from 2 independent experiments, where values denote the numbers of cell division, and redline marks signal levels with isotype control staining.

c,d. Detection of cytokine production by effector CD8$^+$ T cells in recipient spleens during primary response on day 8 after WT, *Tcf7*$^{\Delta Gzmb}$ or *Tcf7*$^{\Delta Gzmb}$*Lef1*$^{\Delta Gzmb}$ P14 CD8$^+$ T

cells were adoptively transferred into CD45.1$^+$ wild-type recipients, followed by LCMV-Arm infection the next day. GP33-induced production of IFN-γ (**c**), TNF and IL-2 (**d**) was detected in CD45.2$^+$CD8$^+$ T cells. Representative contour plots (left) are from ≥3 experiments, with values denoting percentages of the gated population. Cumulative data (right) of the percentage of IFN-γ$^+$ population in P14 CD8$^+$ T cells, IFN-γ relative geometric mean fluorescent intensity (gMFI) (**c**), and the percentage of TNF$^+$ or IL-2$^+$ populations in IFN-γ$^+$ P14 CD8$^+$ T cells (**d**) are means ± s.d.

e. Detection of granzyme B expression in effector CD8$^+$ T cells by intracellular staining on day 8 p.i. Representative histographs (left) are from ≥3 experiments with the values denoting percentage of granzyme B$^+$ cells and those in parentheses denoting gMFI of granzyme B. Cumulative data (left) are means ± s.d. For data in **c**–**e**, statistical significance was first determined with one-way ANOVA for multi-group comparisons, and as post hoc correction, Tukey‟s test was used for indicated pair-wise comparison. *, $p<0.05$; **, $p<0.01$; ***, $p<0.001$; ns, not statistically significant.

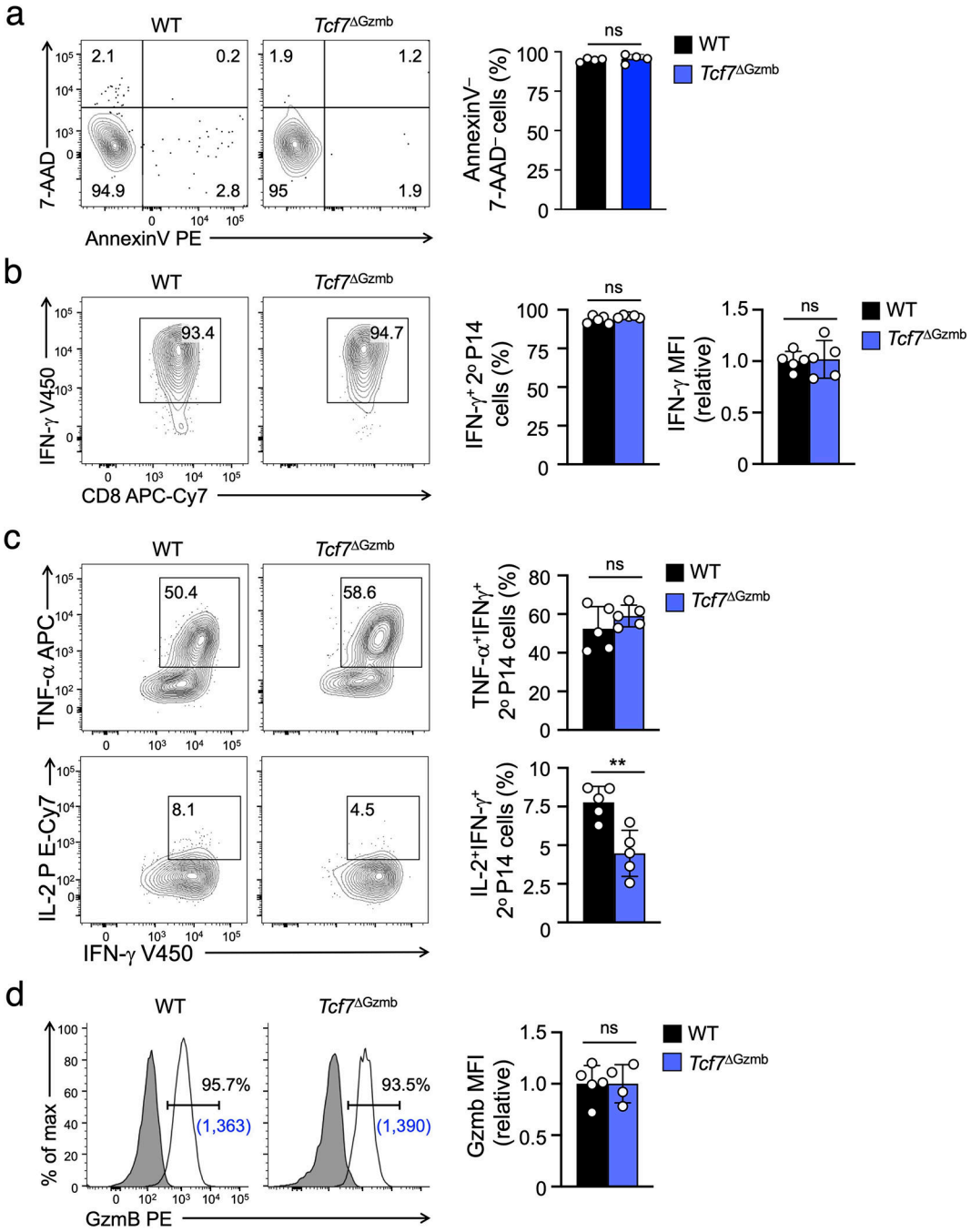

Extended Data Fig. 2. Tcf1 is largely dispensable for induction of cytotoxic effector molecules during CD8$^+$ T$_{cm}$ recall response.

a. Detecting cell viability of early secondary CD8$^+$ T cells in secondary recipients at 60 hrs after CD45.2$^+$ wild-type or *Tcf7*$^{\Delta Gzmb}$ CD62L$^+$CD8$^+$ T$_{cm}$ cells (sorted from the primary recipients on day ≥30–35 p.i., as generated in Fig. 1g) were transferred into CD45.1$^+$ wild-type recipients, which were infected with LCMV-Arm the next day. AnnexinV$^-$7-AAD$^-$ viable cells were detected in CTV$^+$CD45.2$^+$CD8$^+$ T cells, with contour plots (left) from 2 independent experiments, and cumulative data (right) as means ± s.d.

b, c. Detection of cytokine production in secondary effector $CD8^+$ T cells on day 8 after $CD45.2^+$ wild-type or *Tcf7*$^{\Delta Gzmb}$ $CD62L^+CD8^+$ T_{cm} cells (sorted from the primary recipients on day ≥30–35 p.i., as generated in Fig. 1g) were transferred into $CD45.1^+$ wild-type recipients, which were infected with LCMV-Arm the next day. GP33-induced production of IFN-γ (**b**), TNF and IL-2 (**c**) was detected in $CD45.2^+CD8^+$ T cells. Representative contour plots (left) are from 2 independent experiments, with values denoting percentages of the gated population. Cumulative data (right) of the percentage of IFN-γ^+ population in P14 $CD8^+$ T cells, IFN-γ relative gMFI (**b**), and the percentage of TNF^+ or IL-2^+ populations in IFN-γ^+ P14 $CD8^+$ T cells (**c**) are means ± s.d.

d. Detection of granzyme B expression in secondary effector $CD8^+$ T cells by intracellular staining on day 8 p.i. Representative histographs (left) are from 2 independent experiments, with the values denoting percentage of granzyme B^+ cells and those in parentheses denoting gMFI of granzyme B. Cumulative data (left) are means ± s.d. ns, not statistically significant; **, $p<0.01$ as determined with two-tailed Student's *t*-test.

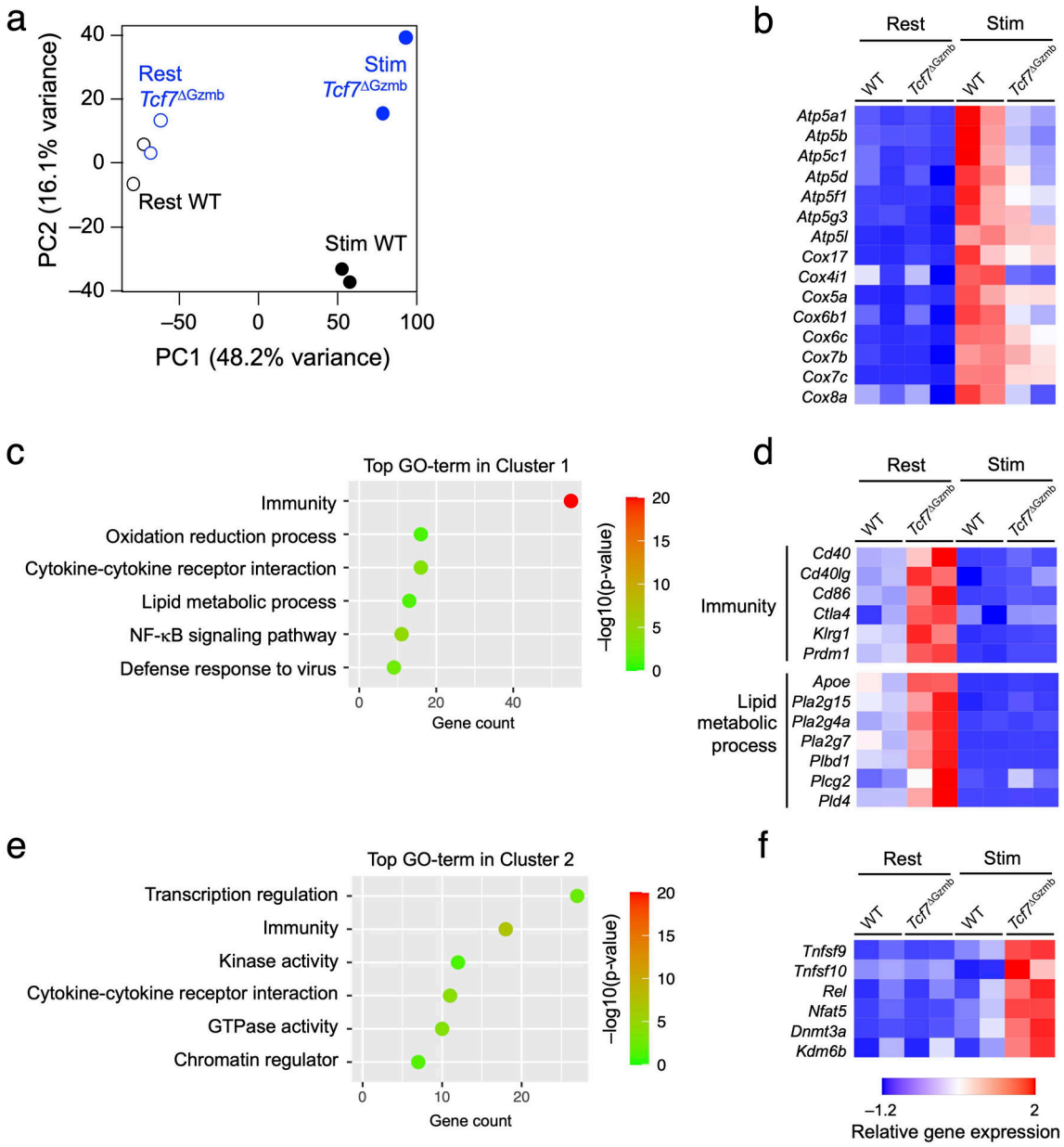

Extended Data Fig. 3. Tcf1 critically regulates transcriptomic changes in CD8$^+$ T$_{cm}$ cells at resting state and after recall stimulation.

a. Principal component analysis (PCA) of the transcriptomes of wild-type or *Tcf7*$^{\Delta Gzmb}$ CD8$^+$ T$_{cm}$ cells at resting state and after 24-hr GP33 stimulation, where log2(RPKM+1) for each gene in different samples were used as the input data.

b,d,f. Heatmaps of select genes involved in “mitochondria” and “oxidative phosphorylation” from Cluster 3+4a (**b**), genes in Cluster 1 (**d**) and Cluster 2 (**f**), with the color represented row-normalized RPM for the genes across different samples.

c,e. Functional annotation of Cluster 1 (**c**) and Cluster 2 (**e**) genes, as defined in Fig. 3e, using DAVID Bioinformatic Resources, with select top gene ontology (GO) terms shown in dot plots and statistical significance denoted with a color scale.

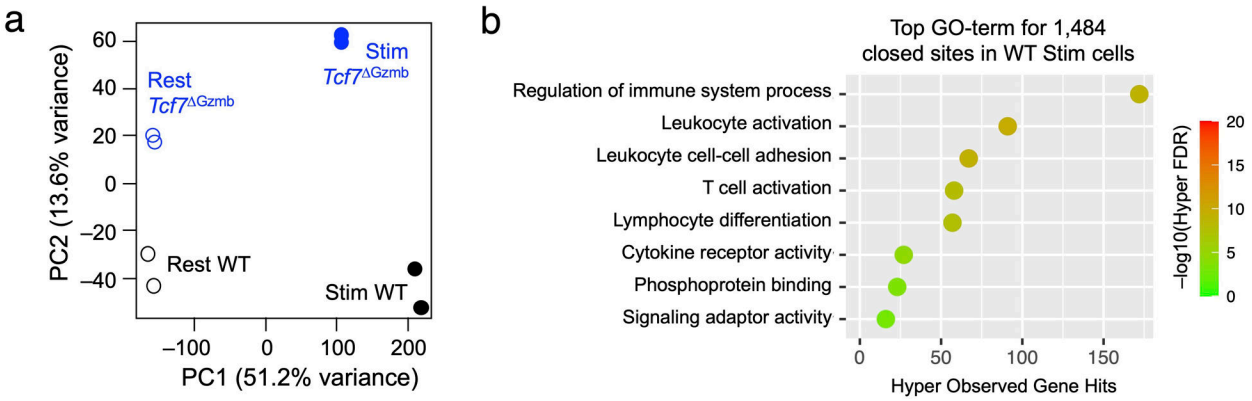

c

Top motifs of 'opened' chromatin sites in GP33-stimulated WT Tcm cells

Motif	Logo	P-value	% of Targets
BATF		1e–3006	34.59
RUNX1		1e–499	26.40
ERG (ETS)		1e–394	17.27
NFKB2		1e–354	4.37
NR2F2		1e–204	17.10
IRF4		1e–199	31.54
BATF:JUN		1e–198	7.15
NFAT:AP1		1e–127	3.87
STAT5		1e–80	3.22
CTCFL		1e–77	1.05

d

Top motifs of 'closed' chromatin sites in GP33-stimulated WT Tcm cells

Motif	Logo	P-value	% of Targets
ETS1		1e–216	38.61
RUNX2		1e–132	34.50
TCF7L2		1e–51	26.48
FOXO3		1e–45	28.64
TBX5		1e–38	21.63

Extended Data Fig. 4. Tcf1 critically regulates chromatin accessibility changes in CD8$^+$ T$_{cm}$ cells at resting state and after recall stimulation.

a. Principal component analysis (PCA) of the ChrAcc profiles of wild-type or *Tcf7*$^{\Delta Gzmb}$ CD8$^+$ T$_{cm}$ cells at resting state and after 24-hr GP33 stimulation, where normalized ATAC-seq signal on merged peaks were used as input data.

b. Functional annotation of recall-'closed' chromatin sites in wild-type CD8$^+$ T$_{cm}$ cells (the 1,484 sites in Fig. 4d) using GREAT analysis, with select top GO terms shown in dot plots and statistical significance denoted with a color scale.

c,d. Motif analysis of recall-'opened" 17,763 (**c**) and –'closed' 1,484 ChrAcc sites (**d**) in GP33-stimulated WT CD8$^+$ T$_{cm}$ cells, as defined in Fig. 4d. Listed are the top transcription factor or hybrid motifs and corresponding logos, along with statistical significance and frequency of occurrence at the target ChrAcc sites.

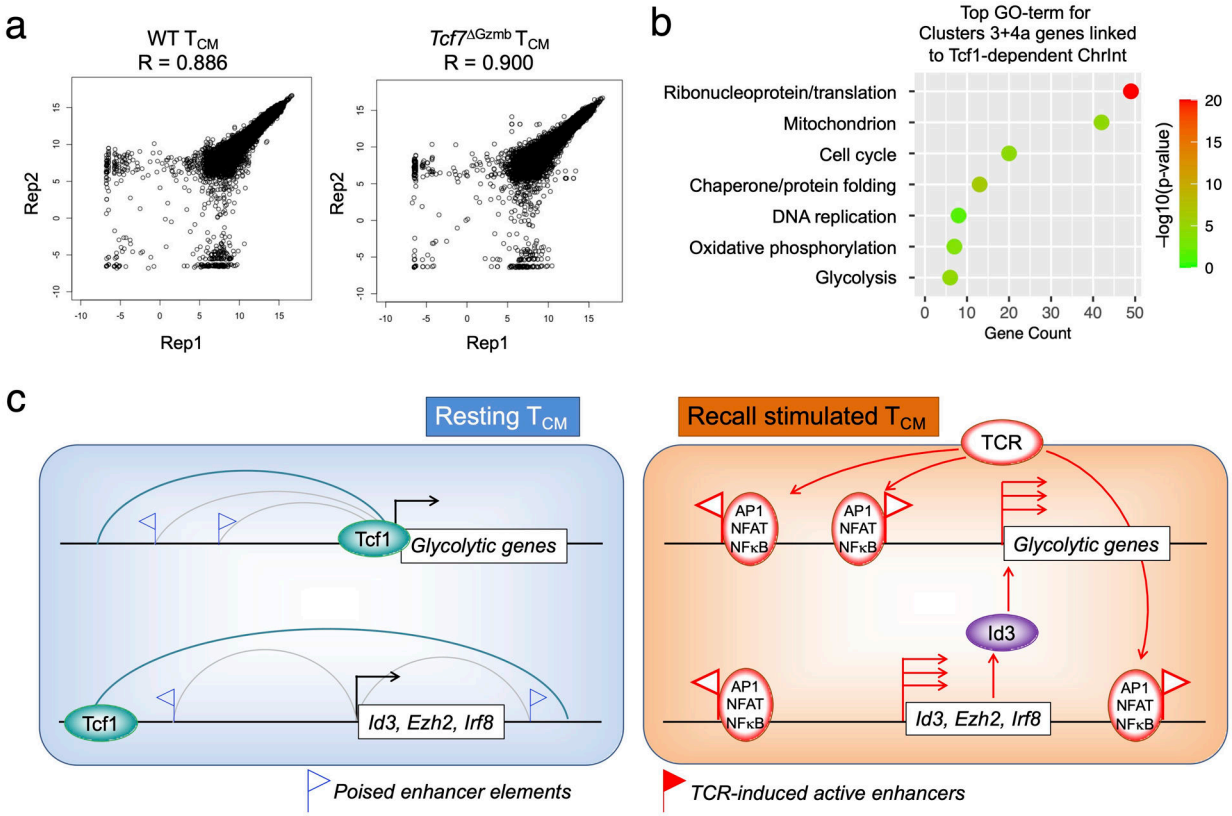

Extended Data Fig. 5. Tcf1 critically regulates chromatin interactions in resting CD8$^+$ T$_{cm}$ cells.

a. Scatterplots showing reproducibility of two biological replicates of Hi-C libraries from resting wild-type or *Tcf7*$^{\Delta Gzmb}$ CD8$^+$ T$_{cm}$ cells. The *x*- and *y*-axis values for each data point (marked with a dot) represent the interaction scores of an anchor in replicate 1 (Rep1) and replicate 2 (Rep2), respectively, and the R values denote Pearson correlation coefficient.

b. Functional annotation of Clusters 3+4a genes associated with Tcf1-dependent Chr.Int. using DAVID, with selected gene ontology (GO) terms shown in dot plots and statistical significance denoted with a color scale.

c. Proposed model for Tcf1-mediated preprogramming of responsiveness of CD8$^+$ T$_{cm}$ cells to recall stimulation. Left, CD8$^+$ T$_{cm}$ cells at resting state express Tcf1 and basal expression of secondary effector CD8$^+$ T cell-associated genes, including transcription regulators such as *Id3* and glycolytic enzymes. In this context, the presence of Tcf1 mediates chromatin interactions that engage the effector gene promoters with distal regulatory regions (top row) or span the effector gene loci (bottom row). The Tcf1-dependent chromatin interactions may thus bring the effector gene promotors and the poised enhancers elements (blue flags) into spatial proximity, which constitutes a 'preprogrammed' state predisposed for transcriptional activation. Right, recall-stimulated CD8$^+$ T$_{cm}$ cells downregulate Tcf1, but TCR-mobilized transcription factors, such as those in the AP-1, NFAT and NF-κB families, increase chromatin accessibility of the poised regulatory elements to become active enhancers (red flags), and hence induce the poised effector genes with higher efficacy. The induced Id3 can further boost activation of glycolytic genes in recall-stimulated CD8$^+$ T$_{cm}$ cells to ensure bioenergetic supplies.

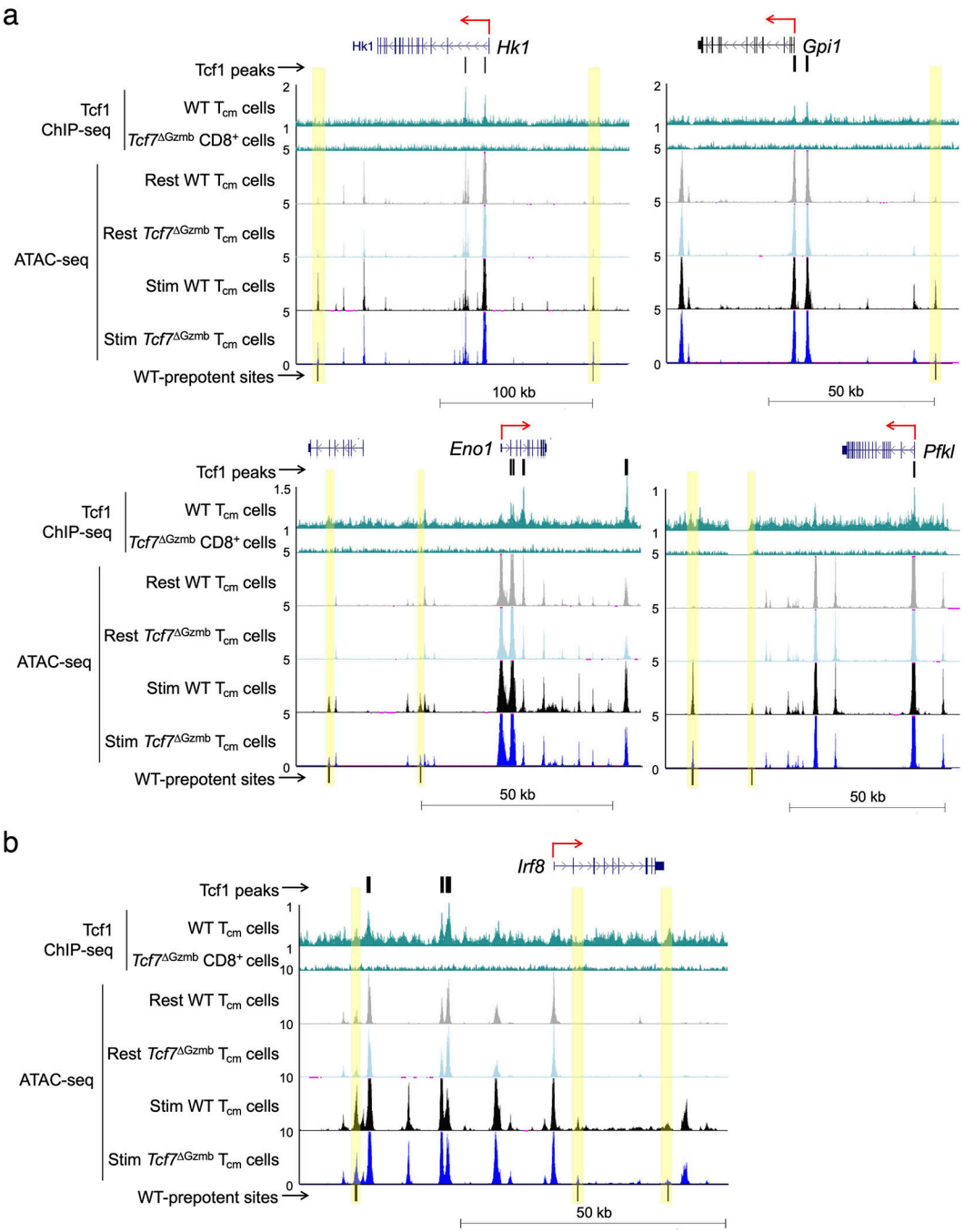

Extended Data Fig. 6. Integrative analysis of Tcf1 occupancy and chromatin accessibility at recall-induced genes in CD8$^+$ T$_{cm}$ cells.

Sequencing tracks at select glycolytic genes (**a**) and *Irf8* (**b**) as displayed on the UCSC genome browser, with gene structure and transcription orientation marked on the top. The tracks included Tcf1 ChIP-seq in WT CD8$^+$ T$_{cm}$ cells and Tcf1-deficient naïve CD8$^+$ T cells, ATAC-seq in resting WT and *Tcf7*$^{\Delta Gzmb}$, and GP33-stimulated WT and *Tcf7*$^{\Delta Gzmb}$ CD8$^+$ T$_{cm}$ cells, where black bars on the top denoted high confidence Tcf1 binding sites and

those at the bottom denoted WT-prepotent (*i.e.*, Tcf1-dependent, recall-"opened") ChrAcc sites with corresponding regions highlighted with yellow vertical bars.

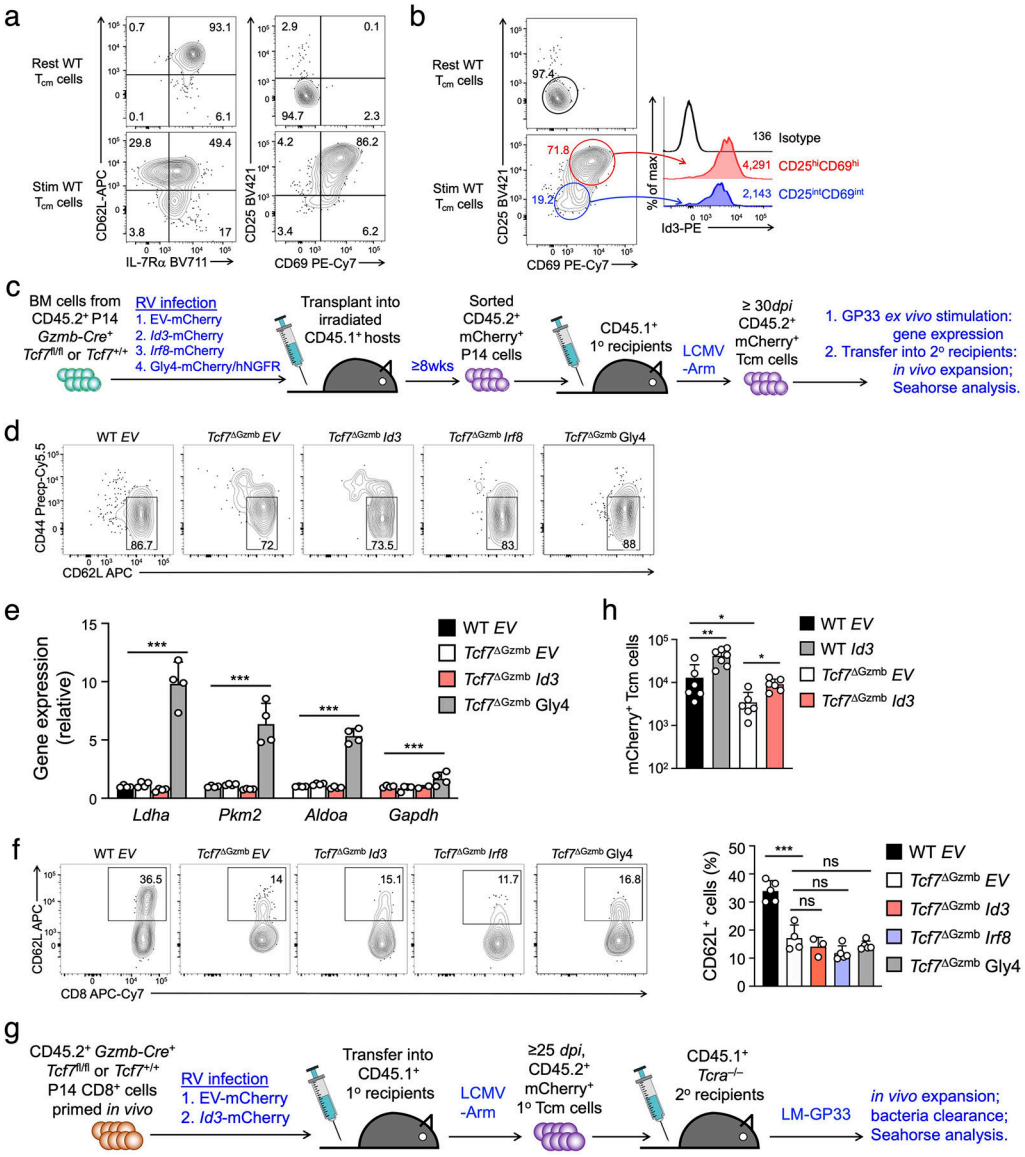

Extended Data Fig. 7. Effect of ectopic expression of select factors on recall responses by CD8$^+$ T$_{cm}$ cells.

a–b. Analysis of cell surface markers (**a**) and Id3 expression (**b**) in CD8$^+$ T$_{cm}$ cells at resting state or after 24-hr GP33 stimulation. Note that recall-induced CD25 and CD69 proteins (right panel in **a**) better demarcated CD8$^+$ T$_{cm}$ cells cell activation than recall-repressed CD62L and IL-7Rα proteins (left panels in **a**). *Sell* and *Il7r* genes were greatly diminished in WT CD8$^+$ T$_{cm}$ cells after 24-hr GP33 stimulation, as detected among the 2,998 genes in Fig. 3b, but their encoded proteins, CD62L and IL-7Rα, remained highly expressed at this time point (left panels), likely due to longer protein half-lives. Data are representative from 3 independent experiments with similar results.

c. Experimental design for 'rescue' studies by gene delivery into BM progenitors. mCherry- or hNGFR-expressing retroviruses were used for gene delivery into CD45.2$^+$ BM progenitors, which were transplanted into irradiatied CD45.1$^+$ wild-type hosts to generate BM chimeras. mCherry$^+$ (hNGFR$^+$) naïve CD8$^+$ T cells were then sorted from the BM chimeras to generate T_{cm} cells, followed by *in vivo* and *ex vivo* analyses.

d. Analysis of cell surface markers in mCherry$^+$ (hNGFR$^+$) CD45.2$^+$CD8$^+$ T cells in the spleens of the BM chimeras reconstituted with BM progenitors infected with mCherry (hNGFR)-expressing retroviruses, where the frequency of CD62L$^+$CD44$^{med\text{-}lo}$ naïve phenotype cells is shown in representative contour plots from 2 independent experiments.

e. Detection of glycolytic gene expression in mCherry$^+$hNGFR$^+$CD8$^+$ T_{cm} cells with RT-PCR at resting state, where the transcripts of each gene were first normalized to *Hprt* in each cell type, and further normalized to resting WT CD8$^+$ T_{cm} cells to calculate the relative expression of the gene in all cell types. Data are mean ± s.d. (n = 4) from 2 independent experiments.

f. Detection of CD62L$^+$CD8$^+$ T_{cm} cell formation in recipient spleens at ≥30 days after CD45.2$^+$ mCherry$^+$ (hNGFR$^+$) naïve P14 CD8$^+$ T cells were sort-purified from the BM chimeras, transferred into CD45.1$^+$ wild-type recipients followed by LCMV infection the next day. The frequency of CD62L$^+$ CD8$^+$ T_{cm} cells is shown in representative contour plots (left) from 2 independent experiments, and cumulative data on CD8$^+$ T_{cm} cell frequency (right) are means ± s.d.

g. Experimental design for 'rescue' studies by gene delivery into CD8$^+$ T cells primed *in vivo*. WT or *Tcf7*$^{\Delta Gzmb}$ P14 transgenic mice were *i.v.* infected with LCMV-Arm to prime P14 CD8$^+$ T cells, which were then infected with mCherry-expressing retroviruses. The retrovirus-transduced cells were transferred into primary recipients to generated CD8$^+$ T_{cm} cells, and the mCherry$^+$ CD8$^+$ T_{cm} cells were then sort-purified for *in vivo* analyses in secondary *Tcra*$^{-/-}$ recipients.

h. Enumerating CD45.2$^+$mCherry$^+$CD8$^+$ T_{cm} cells in the recipient spleens at ≥day 25 after *EV*- or *Id3*-mCherry retrovirus-transduced WT or *Tcf7*$^{\Delta Gzmb}$ P14 CD8$^+$ T cells were transferred into CD45.1$^+$ wild-type recipients, followed by LCMV-Arm infection the next day. Data are means ± s.d. from 2 independent experiments.

Statistical significance for multiple group comparisons in **e**, **f**, and **h** was first determined with one-way ANOVA for multi-group comparison, and Tukey's test was used as post-hoc correction for indicated pair-wise comparisons. ns, not statistically significant; *, $p<0.05$; **, $p<0.01$; ***, $p<0.001$

Supplementary Material

Refer to Web version on PubMed Central for supplementary material.

Acknowledgements

We thank the University of Iowa Flow Cytometry Core facility (J. Fishbaugh, H. Vignes and G. Rasmussen) and the HMH-CDI Flow Cytometry Core facility (M. Poulus and W. Tsao) for cell sorting. This study is supported in-part by grants from the NIH (AI121080 and AI139874 to H.-H.X. and W.P., AI112579 to H.-H.X. and C. Z., GM134880 and AI114543 to V.P.B.). The authors declare no conflict of interests.

Data Availability

The ChIP-seq, RNA-seq, ATAC-seq, and Hi-C data in $CD8^+$ T_{cm} cells are deposited at the Gene Expression Omnibus under accession number GSE177064.

References

1. Martin MD & Badovinac VP Defining Memory CD8 T Cell. Front Immunol 9, 2692 (2018). [PubMed: 30515169]
2. Williams MA & Bevan MJ Effector and memory CTL differentiation. Annu Rev Immunol 25, 171–192 (2007). [PubMed: 17129182]
3. Jameson SC & Masopust D Understanding Subset Diversity in T Cell Memory. Immunity 48, 214–226 (2018). [PubMed: 29466754]
4. Surh CD & Sprent J Homeostasis of naive and memory T cells. Immunity 29, 848–862 (2008). [PubMed: 19100699]
5. Banerjee A et al. Cutting edge: The transcription factor eomesodermin enables CD8+ T cells to compete for the memory cell niche. J Immunol 185, 4988–4992 (2010). [PubMed: 20935204]
6. Zhou X et al. Differentiation and persistence of memory CD8(+) T cells depend on T cell factor 1. Immunity 33, 229–240 (2010). [PubMed: 20727791]
7. Kim MV, Ouyang W, Liao W, Zhang MQ & Li MO The transcription factor Foxo1 controls central-memory CD8+ T cell responses to infection. Immunity 39, 286–297 (2013). [PubMed: 23932570]
8. Utzschneider DT et al. Active Maintenance of T Cell Memory in Acute and Chronic Viral Infection Depends on Continuous Expression of FOXO1. Cell Rep 22, 3454–3467 (2018). [PubMed: 29590615]
9. Laidlaw BJ, Craft JE & Kaech SM The multifaceted role of CD4(+) T cells in CD8(+) T cell memory. Nat Rev Immunol 16, 102–111 (2016). [PubMed: 26781939]
10. Jeannet G et al. Essential role of the Wnt pathway effector Tcf-1 for the establishment of functional CD8 T cell memory. Proc Natl Acad Sci U S A 107, 9777–9782 (2010). [PubMed: 20457902]
11. Hess Michelini R, Doedens AL, Goldrath AW & Hedrick SM Differentiation of CD8 memory T cells depends on Foxo1. J Exp Med 210, 1189–1200 (2013). [PubMed: 23712431]
12. Cui W, Liu Y, Weinstein JS, Craft J & Kaech SM An interleukin-21-interleukin-10-STAT3 pathway is critical for functional maturation of memory CD8+ T cells. Immunity 35, 792–805 (2011). [PubMed: 22118527]
13. Guan T et al. ZEB1, ZEB2, and the miR-200 family form a counterregulatory network to regulate CD8(+) T cell fates. J Exp Med 215, 1153–1168 (2018). [PubMed: 29449309]
14. Roychoudhuri R et al. BACH2 regulates CD8(+) T cell differentiation by controlling access of AP-1 factors to enhancers. Nat Immunol 17, 851–860 (2016). [PubMed: 27158840]
15. Ichii H, Sakamoto A, Kuroda Y & Tokuhisa T Bcl6 acts as an amplifier for the generation and proliferative capacity of central memory CD8+ T cells. J Immunol 173, 883–891 (2004). [PubMed: 15240675]
16. Ji Y et al. Repression of the DNA-binding inhibitor Id3 by Blimp-1 limits the formation of memory CD8+ T cells. Nat Immunol 12, 1230–1237 (2011). [PubMed: 22057288]
17. Zhao X, Shan Q & Xue HH TCF1 in T cell immunity: a broadened frontier. Nat Rev Immunol (2021).
18. Raghu D, Xue HH & Mielke LA Control of Lymphocyte Fate, Infection, and Tumor Immunity by TCF-1. Trends Immunol 40, 1149–1162 (2019). [PubMed: 31734149]
19. Gullicksrud JA, Shan Q & Xue HH Tcf1 at the crossroads of $CD4^+$ and $CD8^+$ T cell identity. Front. Biol 12, 83–93 (2017)
20. Zhao DM et al. Constitutive activation of Wnt signaling favors generation of memory CD8 T cells. J Immunol 184, 1191–1199 (2010). [PubMed: 20026746]
21. He B et al. CD8(+) T Cells Utilize Highly Dynamic Enhancer Repertoires and Regulatory Circuitry in Response to Infections. Immunity 45, 1341–1354 (2016). [PubMed: 27986453]

22. Gullicksrud JA et al. Differential Requirements for Tcf1 Long Isoforms in CD8(+) and CD4(+) T Cell Responses to Acute Viral Infection. J Immunol 199, 911–919 (2017). [PubMed: 28652395]
23. Jameson SC & Masopust D Diversity in T cell memory: an embarrassment of riches. Immunity 31, 859–871 (2009). [PubMed: 20064446]
24. Martin MD et al. Phenotypic and Functional Alterations in Circulating Memory CD8 T Cells with Time after Primary Infection. PLoS Pathog 11, e1005219 (2015). [PubMed: 26485703]
25. Miyagawa F et al. Interferon regulatory factor 8 integrates T-cell receptor and cytokine-signaling pathways and drives effector differentiation of CD8 T cells. Proc Natl Acad Sci U S A 109, 12123–12128 (2012). [PubMed: 22783014]
26. Yang CY et al. The transcriptional regulators Id2 and Id3 control the formation of distinct memory CD8+ T cell subsets. Nat Immunol 12, 1221–1229 (2011). [PubMed: 22057289]
27. He S et al. Ezh2 phosphorylation state determines its capacity to maintain CD8(+) T memory precursors for antitumor immunity. Nat Commun 8, 2125 (2017). [PubMed: 29242551]
28. Shan Q et al. Tcf1 and Lef1 provide constant supervision to mature CD8(+) T cell identity and function by organizing genomic architecture. Nat Commun 12, 5863 (2021). [PubMed: 34615872]
29. Kim BH et al. Benzoxathiole derivative blocks lipopolysaccharide-induced nuclear factor-kappaB activation and nuclear factor-kappaB-regulated gene transcription through inactivating inhibitory kappaB kinase beta. Mol Pharmacol 73, 1309–1318 (2008). [PubMed: 18202307]
30. Verma V et al. MEK inhibition reprograms CD8(+) T lymphocytes into memory stem cells with potent antitumor effects. Nat Immunol 22, 53–66 (2021). [PubMed: 33230330]
31. McLean CY et al. GREAT improves functional interpretation of cis-regulatory regions. Nat Biotechnol 28, 495–501 (2010). [PubMed: 20436461]
32. Grosschedl R, Giese K & Pagel J HMG domain proteins: architectural elements in the assembly of nucleoprotein structures. Trends Genet 10, 94–100 (1994). [PubMed: 8178371]
33. Love JJ et al. Structural basis for DNA bending by the architectural transcription factor LEF-1. Nature 376, 791–795 (1995). [PubMed: 7651541]
34. Lun AT & Smyth GK diffHic: a Bioconductor package to detect differential genomic interactions in Hi-C data. BMC Bioinformatics 16, 258 (2015). [PubMed: 26283514]
35. Pearce EL, Poffenberger MC, Chang CH & Jones RG Fueling immunity: insights into metabolism and lymphocyte function. Science 342, 1242454 (2013). [PubMed: 24115444]
36. O'Neill LA, Kishton RJ & Rathmell J A guide to immunometabolism for immunologists. Nat Rev Immunol 16, 553–565 (2016). [PubMed: 27396447]
37. Pais Ferreira D et al. Central memory CD8(+) T cells derive from stem-like Tcf7(hi) effector cells in the absence of cytotoxic differentiation. Immunity 53, 985–1000 e1011 (2020). [PubMed: 33128876]
38. van der Windt GJ et al. Mitochondrial respiratory capacity is a critical regulator of CD8+ T cell memory development. Immunity 36, 68–78 (2012). [PubMed: 22206904]
39. Danilo M, Chennupati V, Silva JG, Siegert S & Held W Suppression of Tcf1 by Inflammatory Cytokines Facilitates Effector CD8 T Cell Differentiation. Cell Rep 22, 2107–2117 (2018). [PubMed: 29466737]
40. Yu S et al. The TCF-1 and LEF-1 Transcription Factors Have Cooperative and Opposing Roles in T Cell Development and Malignancy. Immunity 37, 813–826 (2012). [PubMed: 23103132]
41. Steinke FC et al. TCF-1 and LEF-1 act upstream of Th-POK to promote the CD4(+) T cell fate and interact with Runx3 to silence Cd4 in CD8(+) T cells. Nat Immunol 15, 646–656 (2014). [PubMed: 24836425]
42. Shan Q et al. Ectopic Tcf1 expression instills a stem-like program in exhausted CD8(+) T cells to enhance viral and tumor immunity. Cell Mol Immunol 18, 1262–1277 (2021). [PubMed: 32341523]
43. Shan Q et al. The transcription factor Runx3 guards cytotoxic CD8(+) effector T cells against deviation towards follicular helper T cell lineage. Nat Immunol 18, 931–939 (2017). [PubMed: 28604718]
44. Kim D, Langmead B & Salzberg SL HISAT: a fast spliced aligner with low memory requirements. Nat Methods 12, 357–360 (2015). [PubMed: 25751142]

45. Pertea M, Kim D, Pertea GM, Leek JT & Salzberg SL Transcript-level expression analysis of RNA-seq experiments with HISAT, StringTie and Ballgown. Nat Protoc 11, 1650–1667 (2016). [PubMed: 27560171]

46. Love MI, Huber W & Anders S Moderated estimation of fold change and dispersion for RNA-seq data with DESeq2. Genome Biol 15, 550 (2014). [PubMed: 25516281]

47. Zhu A, Ibrahim JG & Love MI Heavy-tailed prior distributions for sequence count data: removing the noise and preserving large differences. Bioinformatics 35, 2084–2092 (2019). [PubMed: 30395178]

48. Langmead B & Salzberg SL Fast gapped-read alignment with Bowtie 2. Nat Methods 9, 357–359 (2012). [PubMed: 22388286]

49. Zhang Y et al. Model-based analysis of ChIP-Seq (MACS). Genome Biol 9, R137 (2008). [PubMed: 18798982]

50. Heinz S et al. Simple combinations of lineage-determining transcription factors prime cis-regulatory elements required for macrophage and B cell identities. Mol Cell 38, 576–589 (2010). [PubMed: 20513432]

51. Kulakovskiy IV et al. HOCOMOCO: towards a complete collection of transcription factor binding models for human and mouse via large-scale ChIP-Seq analysis. Nucleic Acids Res 46, D252–D259 (2018). [PubMed: 29140464]

52. Grant CE, Bailey TL & Noble WS FIMO: scanning for occurrences of a given motif. Bioinformatics 27, 1017–1018 (2011). [PubMed: 21330290]

53. Nora EP et al. Molecular basis of CTCF binding polarity in genome folding. Nat Commun 11, 5612 (2020). [PubMed: 33154377]

54. Alavattam KG et al. Attenuated chromatin compartmentalization in meiosis and its maturation in sperm development. Nat Struct Mol Biol 26, 175–184 (2019). [PubMed: 30778237]

55. Durand NC et al. Juicer Provides a One-Click System for Analyzing Loop-Resolution Hi-C Experiments. Cell Syst 3, 95–98 (2016). [PubMed: 27467249]

56. Wang Z, Zhang Y & Zang C BART3D: inferring transcriptional regulators associated with differential chromatin interactions from Hi-C data. Bioinformatics 37, 3075–3078 (2021).

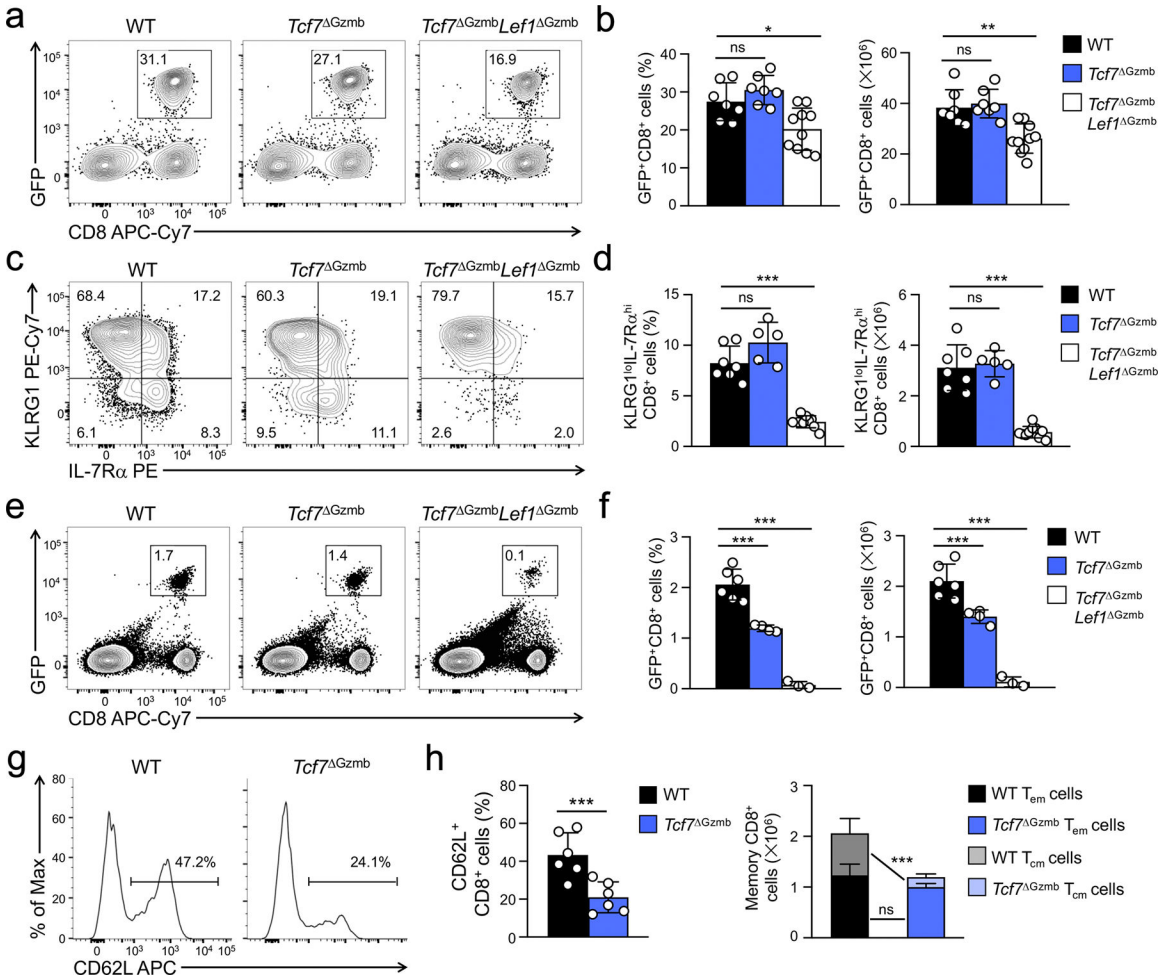

Figure 1. Tcf1 and Lef1 are essential for generating CD8$^+$ memory precursors and T$_{cm}$ cells.

a–b. Frequency (a) and numbers (b) of CD45.2$^+$GFP$^+$ effector CD8$^+$ T cells in recipient spleens on day 8 after transfer of CD45.2$^+$ wild-type (WT), *Tcf7*$^{\Delta Gzmb}$ or *Tcf7*$^{\Delta Gzmb}$*Lef1*$^{\Delta Gzmb}$ CD8$^+$ T cells (2×10^4 each) into CD45.1 WT recipients, followed by infection with LCMV-Arm the next day. **c–d**. Frequency (c) and numbers (d) of KLRG1^{lo}IL-7Rα$^+$ memory precursors in CD45.2$^+$GFP$^+$ effector CD8$^+$ T cells on day 8 p.i. is in a. **e–f**. Frequency (e) and numbers (f) of CD45.2$^+$GFP$^+$ memory CD8$^+$ T cells in recipient spleens at ≥ day 30 p.i. as in a. **g–h**. Frequency (g,h) and numbers (h) of CD62L$^+$ T$_{cm}$ cells in GFP$^+$ memory CD8$^+$ T cells in recipient spleens at ≥ day 30 p.i. Data are representative of 3 (**a**, **c**, **e**), or 2 (**g**) independent experiments. Data in **b**, **d**, **f**, and **h** are cumulative data on cell frequency (left) and numbers (right) as means ± s.d, and n=6 for **h**, or shown as individual data points in all other bar graphs. Statistical significance for multiple group comparisons was first determined with one-way ANOVA for multi-group comparison, and Tukey's test was used as post-hoc correction for indicated pair-wise comparison. Significance in **h** was determined with two-tailed Student's *t*-test. *, p<0.05; **, p<0.01; ***, p<0.001; ns, not statistically significant.

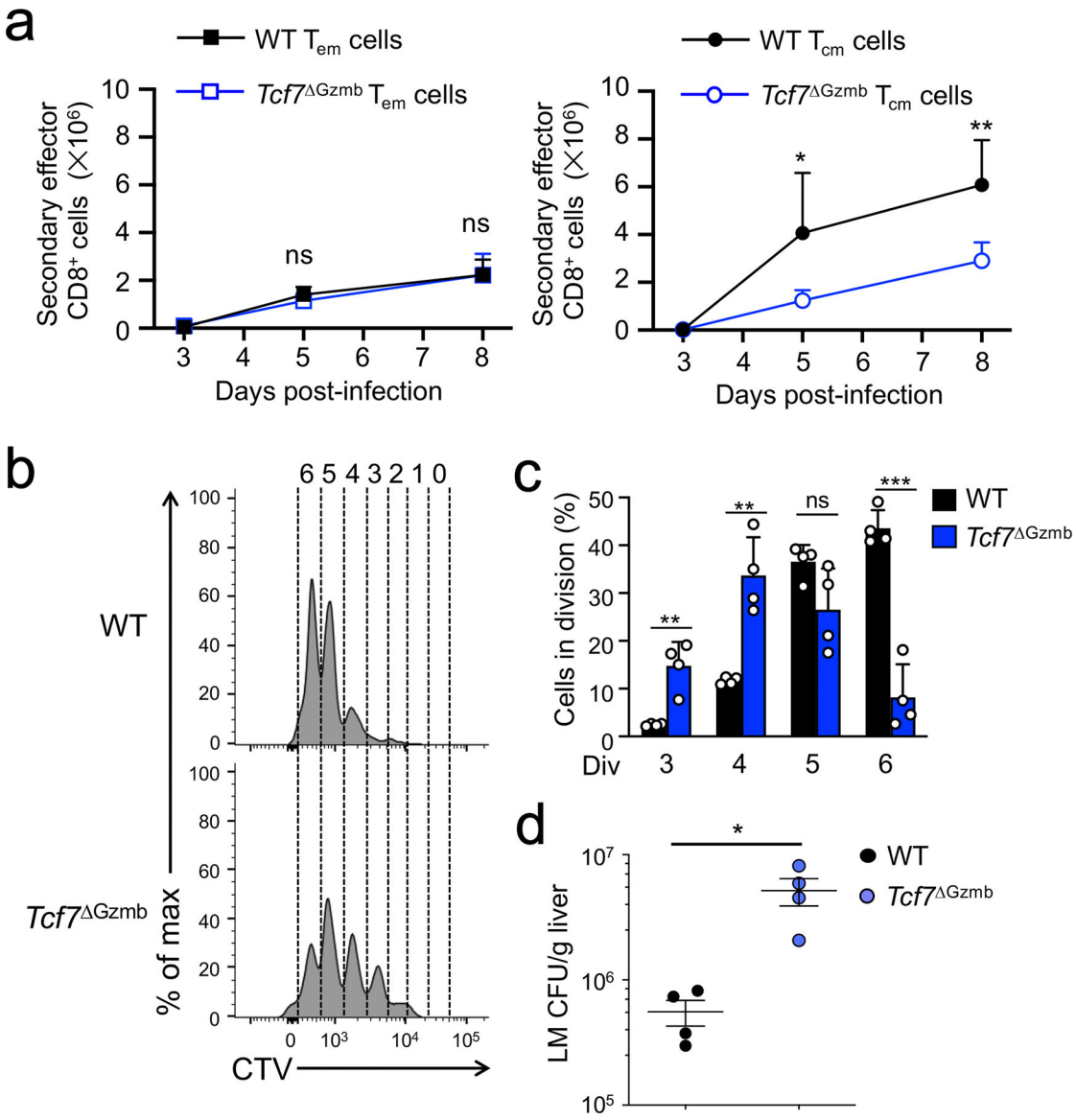

Figure 2. Tcf1 is critical for secondary expansion of $CD8^+$ T_{cm} cells in recall responses.

a. Numbers of secondary effector $CD8^+$ T cells in the recipient spleens on days 3, 5 and 8 after transfer of $CD45.2^+$ WT or $Tcf7^{\Delta Gzmb}$ $CD62L^-CD8^+$ T_{em} (left) or $CD62L^+CD8^+$ T_{cm} cells (right, 500–1,000 cells each, sorted from the primary recipients on day ≥30–35 p.i. as generated in Fig. 1) were transferred into CD45.1 WT recipients, followed by LCMV-Arm infection the next day. **b–c**. Frequency of early cell division of CTV-labeled WT or $Tcf7^{\Delta Gzmb}$ $CD8^+$ T_{cm} cells in secondary recipients at 60 hrs after LCMV-Arm infection, with values in b denoting numbers of cell division. **d**. Bacterial colony formation units (CFUs) in the recipient liver on day 5 after transfer of WT or $Tcf7^{\Delta Gzmb}$ $CD8^+$ T_{cm} cells (2,000 cells each) into $Tcra^{-/-}$ recipients, followed by infection with LM-GP33 the next day. Data in **b** are representative of 2 independent experiments, and those in **a**, **c**, and **d** are cumulative data as means ± s.d. from 2 independent experiments, n=6 for **a**, or shown as

individual data points in other graphs. ns, not statistically significant; *, $p<0.05$; **, $p<0.01$; ***, $p<0.001$ as determined with two-tailed Student's *t*-test.

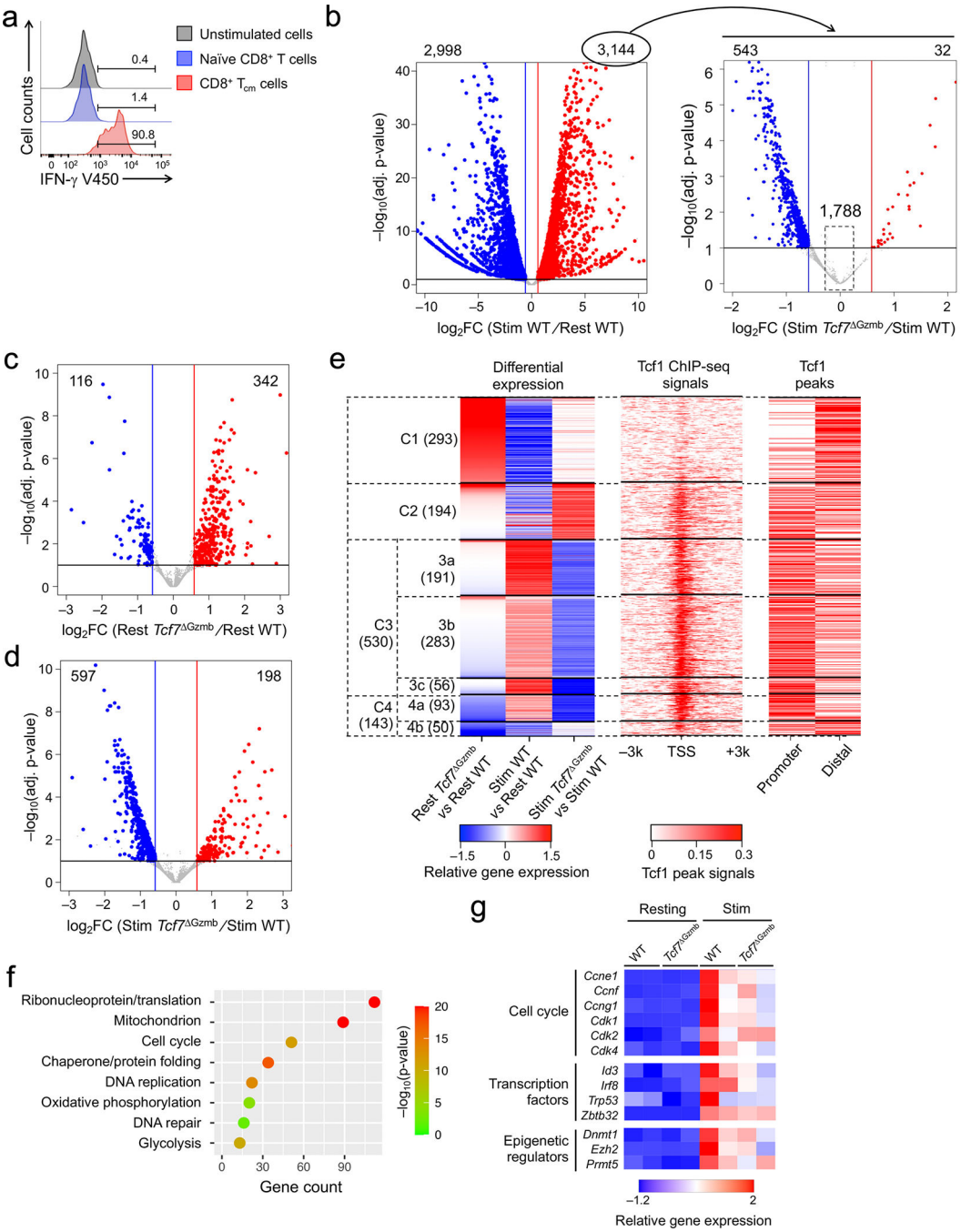

Figure 3. Tcf1 is required for recall-induced transcriptomic changes in CD8$^+$ T$_{cm}$ cells.

a. Production of IFN-γ in CD8$^+$ naïve or T$_{cm}$ cells after 24-hr stimulation with GP33 peptide *ex vivo*. Data are representative from 2 independent experiments. **b–d**. Volcano plots showing differential gene expression changes by RNA-seq in comparisons of GP33-stimulated WT *vs*. resting WT CD8$^+$ T$_{cm}$ (**b**), resting *Tcf7*$^{\Delta Gzmb}$ *vs*. resting WT CD8$^+$ T$_{cm}$ (**c**) and GP33-stimulated *Tcf7*$^{\Delta Gzmb}$ *vs*. GP33-stimulated WT CD8$^+$ T$_{cm}$ (**d**), where values in the plots denote DEG numbers. The GP33-induced 3,144 genes in WT CD8$^+$ T$_{cm}$ cells (b, left) were analyzed for differential gene expression in GP33-stimulated *Tcf7*$^{\Delta Gzmb}$

vs. GP33-stimulated WT $CD8^+$ T_{cm} cells (b, right), where the 1,788 genes had ≤1.2-fold changes and were defined as Tcf1-independent, recall-induced genes. **e**. Left, heatmap showing unsupervised K-means clusters for DEGs from **c** and **d**, using normalized log2 fold change values between two indicated cell states (k=7), with values in parentheses denoting gene numbers in each cluster/subcluster; middle, heatmap showing Tcf1 ChIP-seq signals in resting WT $CD8^+$ T_{cm} cells, with normalized fragment pile-up signals aligned around the TSSs of all DEGs; right, heatmap showing Tcf1 ChIP-seq peak occurrence at promoter (+/−3 kb flanking TSSs) or distal regions (gene body and +/− 50 kb flanking sequence) of DEGs, as marked with horizontal red lines. **f**. Functional annotation of Cluster 3 and Cluster 4a genes using DAVID, with selected gene ontology (GO) terms shown in dot plots and statistical significance denoted with a color scale. **g**. Expression heatmap of selected genes from Cluster 3 and Cluster 4a, with the color representing normalized RPM for each gene across different cell types/states.

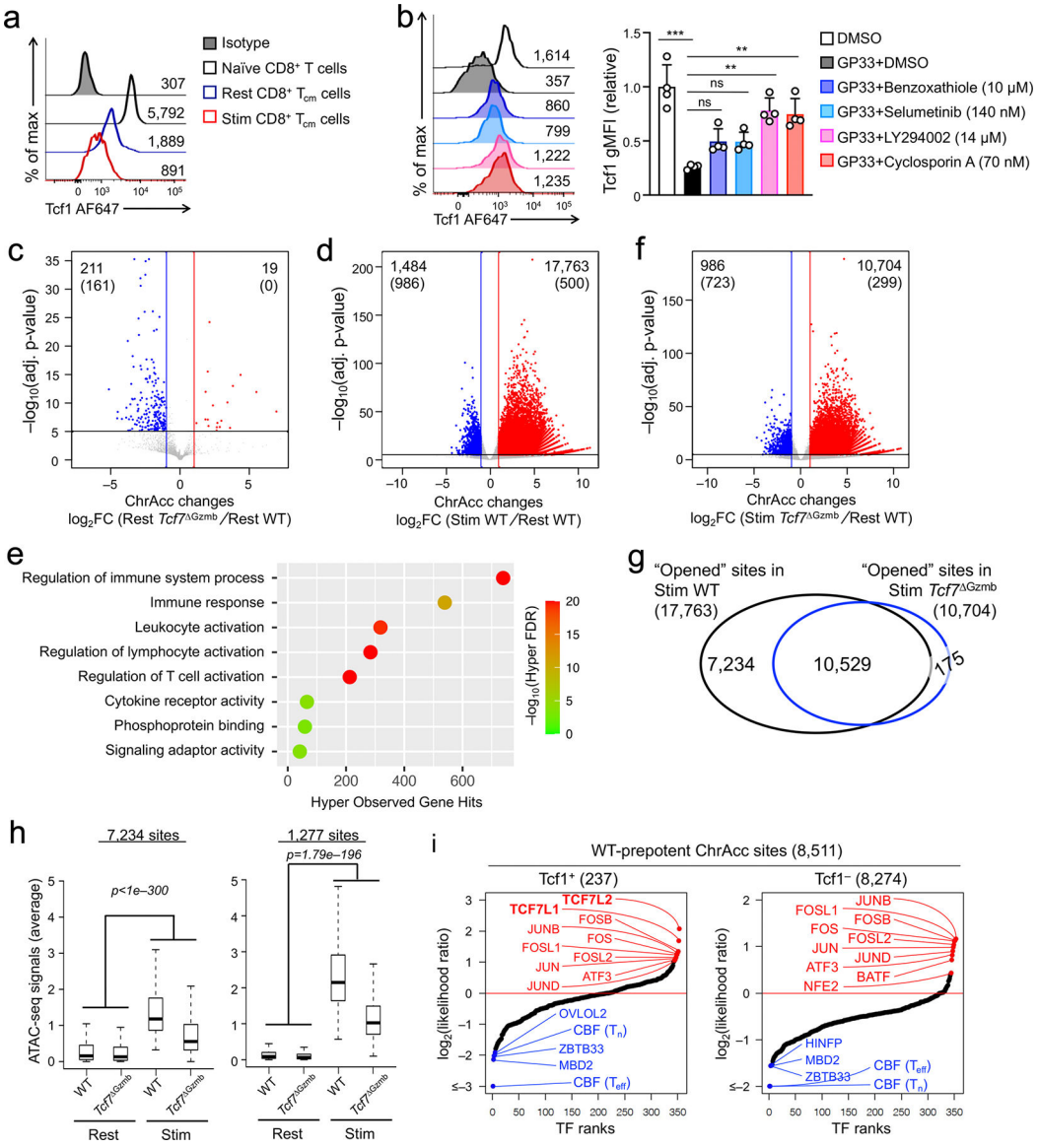

Figure 4. Tcf1 is necessary for recall-induced open chromatin sites in CD8$^+$ T$_{cm}$ cells.

a–b. Tcf1 expression in CD8$^+$ naïve, CD8$^+$ T$_{cm}$ cells at resting state or after GP33 stimulation for 24hrs (a), with DMSO or indicated inhibitors (b), where values in representative half-stacked histographs denote geometric mean fluorescence intensity (gMFI) for Tcf1. Cumulative data in b are means ± s.d. from 2 independent experiments. ns, not statistically significant; **, p<0.01; ***, p<0.001 as determined with two-tailed Student's *t*-test. **c, d, f**. Volcano plots showing ChrAcc changes by ATAC-seq in comparisons of resting *Tcf7*$^{\Delta Gzmb}$ (**c**), GP33-stimulated WT (**d**), or GP33-stimulated *Tcf7*$^{\Delta Gzmb}$ (**f**) CD8$^+$ T$_{cm}$ cells with resting WT CD8$^+$ T$_{cm}$ cells, where values in the plots denote the numbers of differential ChrAcc sites, and those in parentheses denote the numbers of sites overlapping with Tcf1 binding sites. **e**. Functional annotation of recall-'opened' chromatin sites in WT CD8$^+$ T$_{cm}$ cells (17,763 sites in d) using GREAT, with statistical significance denoted with a color scale. **g**. Venn diagram showing numbers

of recall-'opened' chromatin sites in WT and *Tcf7*$^{\Delta Gzmb}$ CD8^{+} T$_{cm}$ cells (*i.e.*, 17,763 sites in d and 10,704 sites in f). **h**. Box plots showing signal strength of WT-prepotent ChrAcc sites using normalized read counts of ATAC-seq peaks in each condition, where left panel represents 7,234 "opened" chromatin sites that were unique in GP33-stimulated WT CD8^{+} T$_{cm}$ cells, and right panel represents 1,277 "opened" chromatin sites that had significantly higher signal strength in GP33-stimulated WT compared to *Tcf7*$^{\Delta Gzmb}$ CD8^{+} T$_{cm}$ cells. The centerlines represent the median, edge of box represents the 25th to 75th percentile range, whiskers represent extreme data points that are no more than 1.5×interquartile range (IQR) from the edge. *P*-values were determined by the one-sided paired Wilcoxon test. **i**. Motif enrichment in Tcf1^{+} and Tcf1^{-} WT-prepotent ChrAcc sites using stable ChrAcc sites as background, where log2 scaled ratio of motif occurrence likelihood between the foreground and background was plotted against transcription factor (TF) ranks, with the top 10 enriched (red) and 5 most depleted (blue) TF motifs marked.

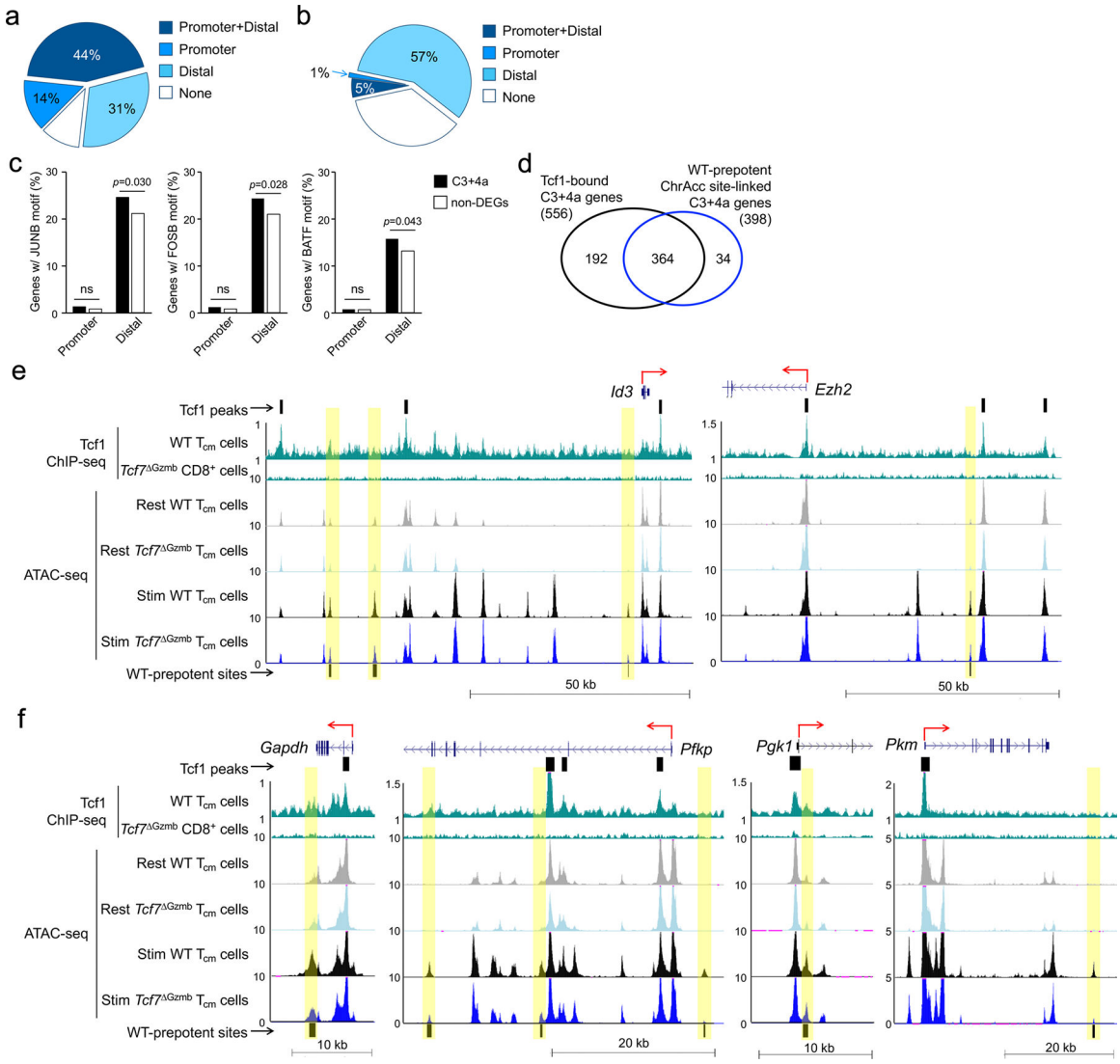

Figure 5. Integrative analysis of recall-induced genes by Tcf1 occupancy and chromatin accessibility.

a. Distribution of Cluster 3 and Cluster 4a genes associated with high confidence Tcf1 binding sites. **b**. Distribution of Cluster 3 and Cluster 4a genes associated with WT-prepotent ChrAcc sites. **c**. Percentage of Cluster 3 and Cluster 4a genes (C3+4a) associated with AP-1 family motifs at their promoters and distal regulatory regions, with direct comparison with non-DEGs between GP33-stimulated and resting WT $CD8^+$ T_{cm} cells. P-values were assessed with the Fisher's exact test. **d**. Venn diagram showing distribution of Cluster 3 and Cluster 4a genes that are linked with Tcf1 binding sites and/or WT-prepotent ChrAcc sites. **e–f**. Sequencing tracks at selected gene loci as displayed on the UCSC genome browser, with gene structure and transcription orientation marked on the top. The tracks included Tcf1 ChIP-seq in WT $CD8^+$ T_{cm} cells and Tcf1-deficient naïve $CD8^+$ T cells, ATAC-seq in resting WT and *Tcf7*$^{\Delta Gzmb}$, and GP33-stimulated WT and *Tcf7*$^{\Delta Gzmb}$ $CD8^+$ T_{cm} cells, where black bars on the top denoted high confidence Tcf1-binding sites and those at the

bottom denoted WT-prepotent (*i.e.*, Tcf1-dependent, recall-“opened”) ChrAcc sites with corresponding regions highlighted with yellow vertical bars.

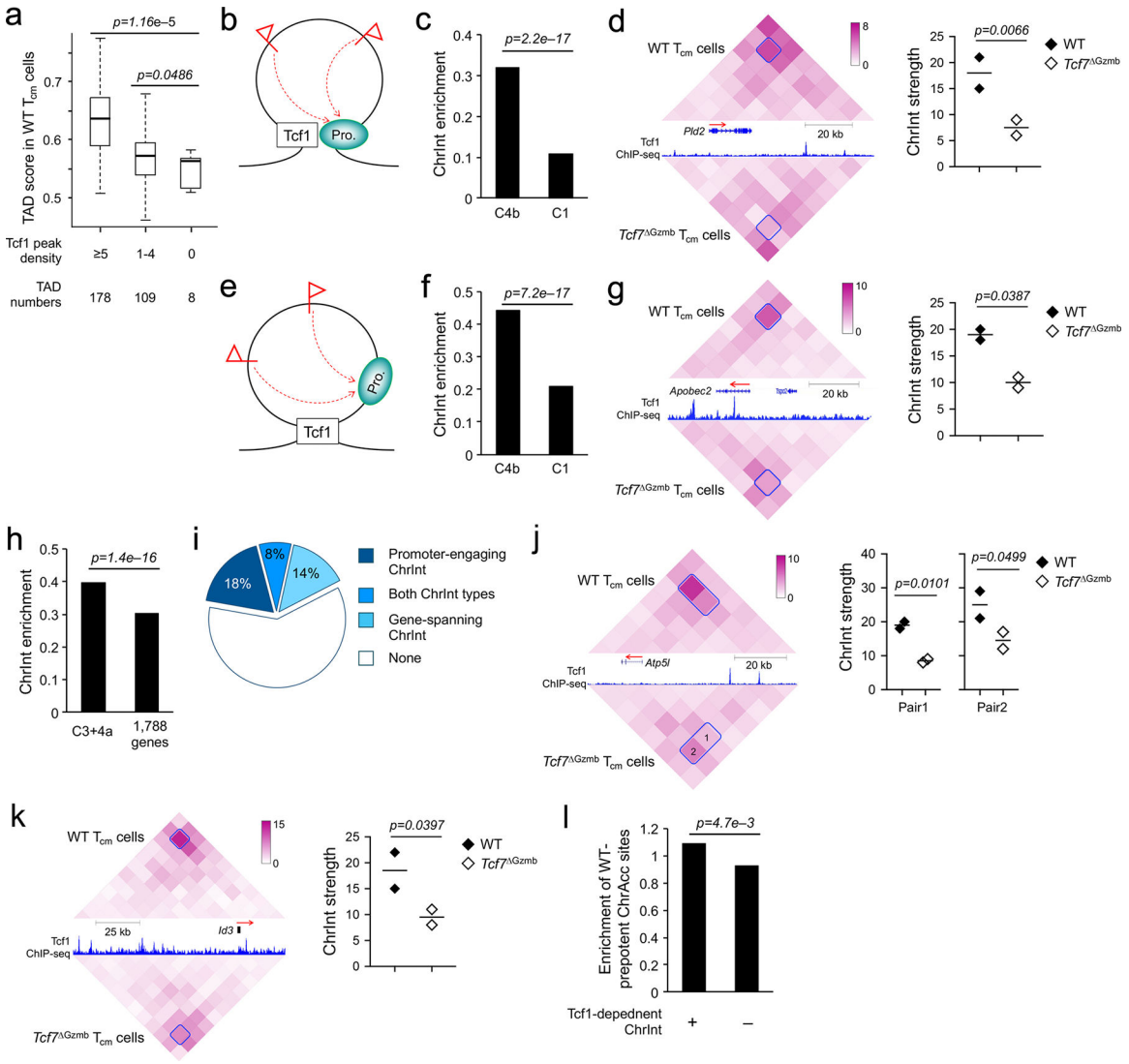

Figure 6. Tcf1 mediates chromatin interactions to control CD8$^+$ T$_{cm}$ gene expression at resting and recall-stimulated states.

a. TAD scores in different groups based on Tcf1 peak numbers per 100 kb in WT CD8$^+$ T$_{cm}$ cells. Centerlines represent median, edge of box represents 25th-75th percentile range, whiskers represent extreme data points ≤ 1.5×IQR from the edge, *p*-values by one-sided paired Wilcoxon-test. **b**. Diagram illustrating the scenario that Tcf1 mediated chromatin interactions (ChrInt) that engaged promoters with distal regions, where red flags denoted active or poised enhancers. Pro., promoter. **c**. Enrichment of Tcf1-dependent, promoter-engaging ChrInt in Tcf1-activated Cluster 4b and Tcf1-repressed Cluster 1 genes (defined in Fig. 3e) in resting CD8$^+$ T$_{cm}$ cells. **d, g**. Diamond graph (left) showing the strength of ChrInt that connected the *Pld2* promoter and a Tcf1-bound distal region (d) and that spanned the *Apobec2* gene (g) in WT and *Tcf7*$^{\Delta Gzmb}$ CD8$^+$ T$_{cm}$ cells, as marked with blue boxes. The distance-normalized Hi-C read counts are summarized as ChrInt strength in dot plots (right). **e**. Diagram illustrating the scenario that Tcf1 mediated ChrInt that spanned gene promoters and regulatory elements. **f**. Enrichment of Tcf1-dependent, gene-spanning ChrInt

in Tcf1-activated Cluster 4b and Tcf1-repressed Cluster 1 genes in resting $CD8^+$ T_{cm} cells. **h**. Enrichment of Tcf1-dependent ChrInt in Tcf1-depenent, recall-induced genes (marked as C3+4a as defined in Fig. 3e) and the 1,788 Tcf1-independent, recall-induced genes (defined in Fig. 3b, right panel). **i**. Distribution of Cluster 3 and Cluster 4a genes associated with Tcf1-dependent promoter-engaging and/or gene-spanning ChrInt. **j–k**. Diamond graph (left) showing the strength of ChrInt that connected the *Atp5l* gene and a Tcf1-bound distal region (j) and that spanned the *Id3* gene (k) in WT and *Tcf7*$^{\Delta Gzmb}$ $CD8^+$ T_{cm} cells, as marked with blue boxes, with distance-normalized Hi-C read counts are summarized as ChrInt strength (right). **l**. Enrichment of WT-prepotent ChrAcc sites in C3+4a genes associated with Tcf1-dependent ChrInt than those without. Statistical significance was determined using one-sided Mann-Whitney U test (**a**), one-sided binomial test (**c**, **f**, **h**), one-sided Poisson test (**l**), and that for **d**, **g**, **j**, and **k** was determined in the diffHiC algorithm.

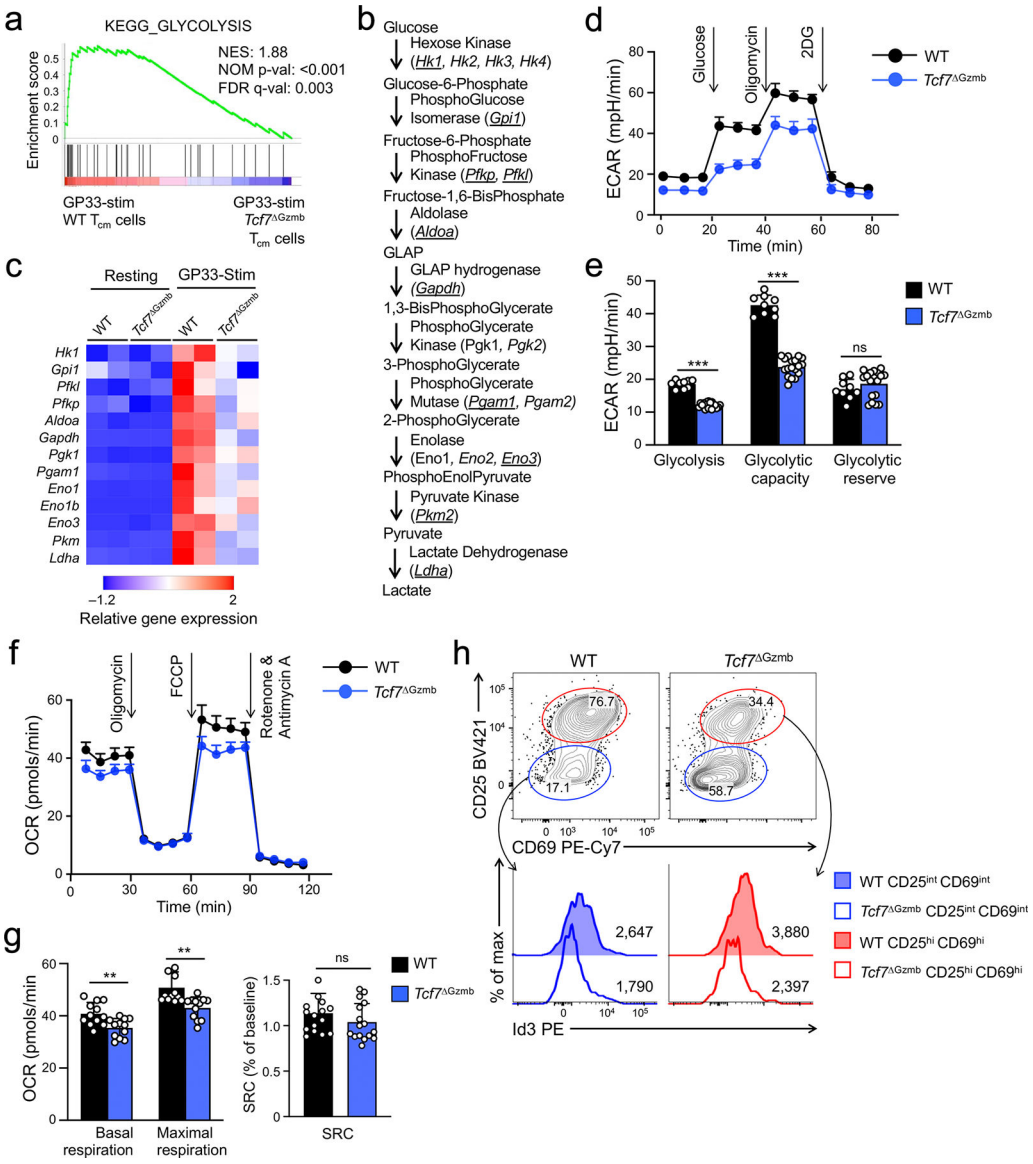

Figure 7. Tcf1 preprograms recall-induced activation of glycolysis in CD8$^+$ T$_{cm}$ cells.

a. Enrichment plot for "KEGG_GLYCOLYSIS" gene set in comparison of GP33-stimulated WT *vs.* *Tcf7*$^{\Delta Gzmb}$ CD8$^+$ T$_{cm}$ cell transcriptomes with GSEA. NES, normalized enrichment score; NOM p-val, nominal P values; FDR q-val, false discovery rate q values. **b**. Diagram showing all glycolysis steps, along with the metabolic enzymes and corresponding genes, where underlined genes were found in Cluster 3 or Cluster 4a. **c**. Expression heatmap of glycolytic genes, with the color representing normalized RPM for each gene across different cell types/states. **d–g**. Profiles of key glycolysis (d,e) and mitochondrial respiration (f,g) parameters determined with the Seahorse Extracellular Flux Analyzer in secondary effector CD8$^+$ T cells in the recipient spleens on day 5 after transfer of CD45.2$^+$ WT or *Tcf7*$^{\Delta Gzmb}$ CD8$^+$ T$_{cm}$ cells (500–1,000 cells each, sorted from the primary recipients on day ≥30–35 p.i. as in Fig. 1) into CD45.1 WT recipients, followed by LCMV-Arm infection the next day. Seahorse traces of ECAR measurements (d) at baseline and after treatment with glucose,

oligomycin (Oligo) and 2-DG, and those of OCR measurements (f) at baseline and after treatment with oligomycin, FCCP and Retenone+Antimycin A. Cumulative data on ECAR (e), basal and maximum OCR, and SRC (calculated as ratio of FCCP-elicited OCR to basal OCR) (g) are are means ± s.d. from 2 independent experiments. ns, not statistically significant; **, $p<0.01$; ***, $p<0.001$ as determined with two-tailed Student's *t*-test. **h**. Distribution of $CD25^{hi}CD69^{hi}$ and $CD25^{int}CD69^{int}$ subsets in WT and *Tcf7*$^{\Delta Gzmb}$ $CD8^{+}$ T_{cm} cells after 24-hr GP33 stimulation (top), and Id3 expression in each subset (bottom, values denoted gMFI for Id3). Data are representative from 2 independent experiments.

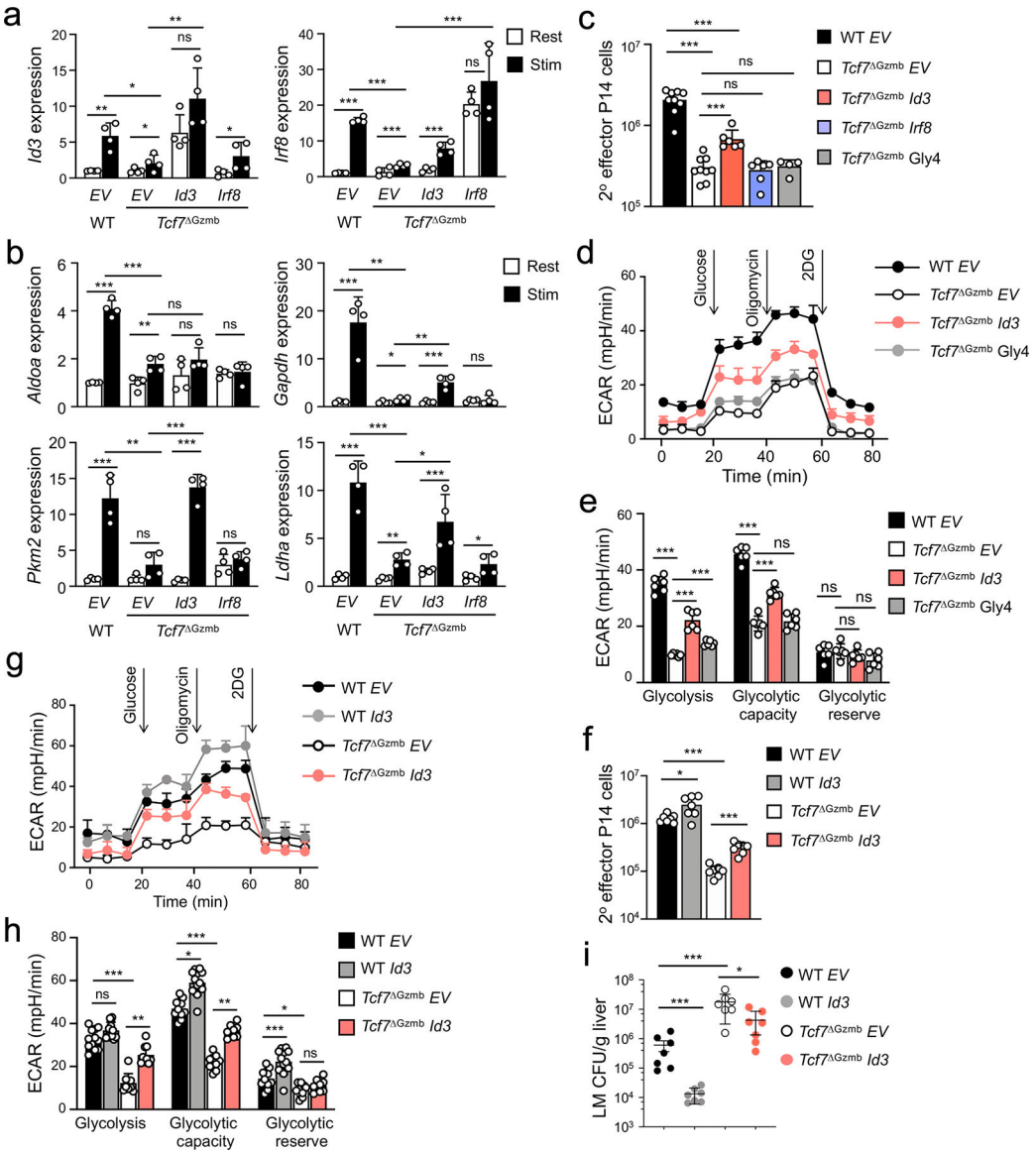

Figure 8. Tcf1 acts upstream of Id3 induction to promote CD8$^+$ T$_{cm}$ recall response.

a–b. Gene expression by RT-PCR in mCherry$^+$(hNGFR$^+$) WT or *Tcf7*$^{\Delta Gzmb}$ CD8$^+$ T$_{cm}$ cells (generated following protocol in Extended Data Fig. 7c) before or after 24-hr GP33 stimulation *ex vivo*, where the transcripts of each gene were first normalized to *Hprt* in each cell type, and further normalized to resting WT mCherry$^+$CD8$^+$ T$_{cm}$ cells to calculate the relative expression of the gene in all cell types. **c**. Numbers of effector CD8$^+$ T cells in recipient spleens at day 8 after transfer of CD45.2$^+$mCherry$^+$(hNGFR$^+$) WT or *Tcf7*$^{\Delta Gzmb}$ CD8$^+$ T$_{cm}$ cells into CD45.1 WT recipients followed by LCMV-Arm infection the next day. **d–e**. Profile of glycolysis parameters of mCherry$^+$(hNGFR$^+$) CD8$^+$ T$_{cm}$ cell-derived secondary effector CD8$^+$ T cells generated *in vivo* on day 5 post-infection with LCMV-Arm, with Seahorse traces showing ECAR (d). **f**. Numbers of effector CD8$^+$ T cells in recipient spleens at day 5 after transfer of CD45.2$^+$mCherry$^+$ WT or *Tcf7*$^{\Delta Gzmb}$ CD8$^+$ T$_{cm}$ cells (generated following protocol in Extended Data Fig. 7g) into *Tcra*$^{-/-}$recipients followed

by LM-GP33 infection the next day. **g–h**. Glycolysis parameters of mCherry^{+} CD8^{+} T_{cm} cell-derived secondary effector CD8^{+} T cells generated *in vivo* on day 5 post-infection with LM-GP33, with Seahorse traces showing ECAR (g). **i**. LM-GP33 CFUs in the recipient liver on day 5 after LM-GP33 infection. Cumulative data in **a**, **b**, **c**, **e**, **f**, and **h** are means ± s.d. from 2 independent experiments. ns, not statistically significant; *, $p<0.05$; **, $p<0.01$; ***, $p<0.001$ as determined with two-tailed Student's *t*-test.